NASICON-based all-solid-state Na-ion batteries: A perspective on manufacturing via tape-casting process

Hasegawa, George
Institute of Materials and Systems for Sustainability, Nagoya University

Hayashi, Katsuro
Department of Applied Chemistry, Graduate School of Engineering, Kyushu University

出版情報：APL Energy. 1 (2), pp.020902-, 2023-07-05. AIP Publishing
バージョン：

NASICON-based all-solid-state Na–ion batteries: A perspective on manufacturing via tape-casting process

Cite as: APL Energy 1, 020902 (2023); doi: 10.1063/5.0151559
Submitted: 23 March 2023 • Accepted: 30 May 2023 •
Published Online: 5 July 2023

George Hasegawa[1,a] and Katsuro Hayashi[2]

AFFILIATIONS

[1] Institute of Materials and Systems for Sustainability, Nagoya University, Furo-cho, Chikusa-ku, Nagoya 464-8601, Japan
[2] Department of Applied Chemistry, Graduate School of Engineering, Kyushu University, 744 Motooka, Nishi-ku, Fukuoka 819-0395, Japan

[a] **Author to whom correspondence should be addressed:** h-george@imass.nagoya-u.ac.jp.
Tel.: +81 52 789 5859/**Fax:** +81 52 789 3920

ABSTRACT

On the background of the urgent demand to realize a decarbonized society, energy storage technology plays a key role in shifting from social activities founded on the combustion of fossil fuels to those based on renewable energy resources. Toward this end, global deployment of large-scale rechargeable batteries supplying electricity to power grids is imperative, which requires widespread commercialization of high-performance and safe batteries at a low price relying on abundant and ubiquitous source materials and a cost-efficient manufacturing process. Along this line, the trend of the battery research field is currently located at a turning point: "from Li–ion to Na–ion" and "from liquid to solid electrolyte." From the viewpoints of the distinguished oxide solid electrolyte, Na superionic conductor (NASICON), and the long-standing progress in ceramic processing, Na–ion all-solid-state batteries (Na-ASSBs) based on NASICON and its derivatives show great promise to realize an innovative and sustainable society in the future. At this moment, however, Na-ASSBs face multifaceted and formidable challenges to overcome for practical usage, mostly relating to interfacial matters in terms of interparticle and interlayer contacts. Here, we overview the recent research progress in NASICON-based solid electrolytes (SEs) from the aspects of synthetic techniques and sintering aids, particularly focusing on the tape-casting process and glass additive. We also provide insights into how to prepare electrode layers and incorporate them with an SE layer into an ASSB cell via tape casting, with the prospect of a high-capacity multilayer-stacked ASSB analogous to the multilayer ceramic capacitors (MLCCs). In addition, the feasibility of a Na metal anode in conjunction with the NASICON-type SEs and the tape-casting process toward an MLCC-type cell configuration is discussed. In the last section, we propose our ideas about future research directions in relevant fields to achieve a breakthrough for Na-ASSBs based on NASICON.

I. INTRODUCTION

The advent of rechargeable "lithium–ion" batteries (LIBs) in the market, pioneered by Sony Corp.[1–4] after the abortion of rechargeable "lithium" battery (Molicel®) supplied by Moli Energy, Ltd.,[5] brought noticeable innovation to not only energy storage applications but also all the relevant fields such as electronics.[6,7] The marked miniaturization of various portable devices that has continued up until now is undoubtedly associated with the evolution of small power sources with high power and energy densities. Continuous efforts to improve the longevity and safety of LIBs have enabled the deployment of large-scale LIBs for electric/hybrid electric vehicles (EVs/HEVs) and stationary storage in the last decade.[8–11] However, in the context of the current environmental crisis of global warming and frequent climatic anomalies predominantly posed by a large quantity of CO_2 emissions as a result of energy generation derived from fossil fuel combustion, a new type of rechargeable battery that surpasses the incumbent LIBs in terms of safety and cost while holding an acceptable energy density is urgently demanded. This is because, in order to realize an

environmentally benign and sustainable energy infrastructure with no or little reliance on fossil fuels, the electricity generation from renewable sources needs to be combined with a large-scale energy storage system due to the intermittent nature of solar and wind power and the shortage of hydroelectric power plants to fulfill the world's electricity consumption: storing excess energy, for example, harvested electricity during low usage or high production, and supplying it to the power grid when the demand exceeds the production rate.[10–13] In this regard, it is implausible that conventional LIBs based on an organic liquid electrolyte can afford such grid-scale energy storage over the world from the viewpoint of the insufficient and localized Li sources within the Earth's crust, inevitably resulting in a high production cost.[14] Recycling discarded LIBs might be a possible solution to the scarcity issue for Li and other constituting elements, while the relevant technology is, as of yet, in a very early stage and far from the practical level.[15–18]

The use of Na–ion chemistry, i.e., sodium–ion batteries (SIBs), is a promising and viable choice owing to the wealth of Na resources.[19–24] As the cost of manufacturing a cell is dominated by the prices of the materials,[25] significant cost savings are expected for producing SIBs compared with LIBs when electrode active materials based on abundant and accessible elements like Ti, Fe, and Mn are adopted together with the omnipresent Na. However, SIBs with an organic liquid electrolyte sacrifice safety by increasing the risk of serious hazards due to the higher reactivity of Na than that of Li when a dendritic precipitate forms. All-solid-state batteries (ASSBs),[26–36] in which an ion-conducting solid layer plays the roles of both separator and electrolyte, offer a solution for the safety concerns suffering from the underlying flammability and explosibility of an organic liquid electrolyte. There exists another advantage that ASSBs have a chance to implement cathode candidates that are not adoptable to conventional liquid-electrolyte type batteries due to inherent issues such as too high operating potential above the potential window of liquid electrolytes and solubility in liquid electrolytes like Mn-based active materials.[37–42] In addition, oxide-based solid electrolytes (SEs) can confer availability over a wide temperature range owing to their high thermal stability. In this sense, ASSBs using Na^+ ions as a charge carrier (Na-ASSBs) are regarded as the leading candidate for a next-generation battery to address both safety and cost concerns and thereby enable large-quantity and/or large-scale energy storage systems to be deployed worldwide.

However, the replacement of a liquid electrolyte with a solid alternative imposes several challenges to producing a practically usable ASSB that can be operated with sufficient energy density at a reasonable current density. While it is essential to achieve efficient transport of charge carriers within the anode and cathode layers, as is the case with conventional batteries with a liquid electrolyte, the crux of ASSBs is how to establish smooth pathways of cations across a monolithic cell (most simply, a tri-layer laminate of anode|SE|cathode) involving grain boundaries and electrode/electrolyte interfaces.[29,33,35,43–45] Since most active electrode materials show relatively low ionic conductivity, SE particles are often incorporated into electrode layers. It is, therefore, indisputable that the most vital component in ASSBs is the SE, which determines the cell's performance with respect to energy density, rate capability, and cycle stability. Accordingly, a great deal of research effort has been devoted to developing ion-conducting solids for SEs to date, which are classified into three categories: organic polymer electrolytes,[46,47] inorganic SEs,[48–54] and their composites.[50,53,55] Each class of SEs has its pros and cons, which need to be weighed depending on the type of ASSBs for the intended application (small or large; flexible or rigid; low-rate or high-rate charge/discharge; operating temperature range).

The organic polymer electrolytes are characterized by a flexible mechanical feature capable of readily making a good interface with an electrode layer, yet suffer from several drawbacks, including poor ionic conductivity along with a low cationic transference number (typically, $t_+ < 0.5$) due to the large contribution of anion migration, a narrow electrochemical stability window, and a limited range of operational temperature.[46,47] The composite SEs, which combine the features of polymer electrolytes and inorganic SEs, show enhanced ionic conductivity while maintaining a flexible nature.[50,53,55] Nevertheless, this emerging class of electrolyte materials still has room for improvement in ionic conductivity, transference number, and electrochemical stability to satisfy the requirements for practical use.

By contrast, the notable advantage of inorganic SEs lies in their high ionic conductivity ($>10^{-4}$ S cm^{-1} at room temperature) together with a cationic transference number close to unity, which enables fast ionic transportation comparable with or even faster than that in an organic liquid electrolyte.[56–58] The major groups of inorganic SEs are sulfide- and oxide-based ion conductors.[48–53] The former SEs have the advantage over the latter in terms of plasticity, which allows for not only facile densification of the SE layer but also intimate contact between the SE and electrode active particulates by a single-step mechanical compression even without heating.[59–61] Despite this immense benefit, the sulfide-based SEs are notoriously plagued by critical deficits: poor stability against moisture and, what is more, the evolution of toxic H_2S gas on decomposing sulfide SEs, which spoils the superiority in the safety of ASSBs. Therefore, to reconcile this dilemma, non-sulfide inorganic SEs imbued with high ionic conductivity as well as plasticity have been developed recently, as represented by a group of borohydride salts.[54,62–68] However, technologies for economically viable mass production of borohydride-based SEs have yet to be established.

On the other hand, the oxide-based SEs are characterized by high thermodynamic stability and a wide bandgap, leading to a wide electrochemical stability window and processability under atmospheric conditions. It indicates that well-developed slurry-based ceramic processing technologies are available, affording large-scale and low-cost production of ASSBs.[69–73] In addition, the high safety of ASSBs imparted by the oxide-based SEs is valuable for aerospace applications since hazard risks must be thoroughly obviated in such situations.

The oxide-based SEs, however, encounter daunting challenges when assembled into ASSBs, which are incurred by their high elastic moduli and, thereby, extremely poor plasticity.[74] This drawback makes it cumbersome to densify an SE layer and elaborate intimate contact with a large area between SE and electrode active materials. The low ductility of oxides is also problematic for guaranteeing a long cycle life since intimate contact, even when successfully established in production, is prone to being spoiled by the volume change of active materials during charge/discharge.[32,35,75–78] So far, several approaches to circumventing these issues have been proposed, most

of which resort to wetting aids such as ionic liquids, polymer electrolytes, and other plastic SEs.[33,35,43,45,79–85] However, these strategies compromise the essential advantages of oxide-based ASSBs including high safety.[86] In another way, the incremental development of ceramic processing technologies is expected to provide a complete solution for materializing real ASSBs based solely on oxide-based SEs.

Among the manufacturing methodologies of ceramics, tape casting is a mature process with ~80 years of history[87–90] and is suitable for producing ASSBs owing to its versatility to produce diverse ceramic sheets and laminates with a controlled thickness and the feasibility of large-scale production at a reasonable cost,[71,72] which is of significance for the shift from laboratory to industry. Indeed, the ceramic products commercialized thus far relying on tape-casting technology literally underpin today's human society: e.g., multi-layer ceramic capacitors (MLCCs) as one of the key components of electronic devices,[91–94] oxygen gas sensors for automobile exhaust emission control systems,[95] and solid oxide fuel cells (SOFCs),[96–98] which are now regarded as a flagship electric power co-generator for housings, office buildings, and plants. These devices have a multi-layer configuration as with ASSBs, indicating that the existing facilities and know-hows for their production can be transferred to manufacturing ASSBs partially or wholly. This prospect is proved in the case of Li–ion ASSBs: some ceramic manufacturers, viz., TDK Corp., Taiyo Yuden Co., Ltd., and Murata Manufacturing Co., Ltd., which are renowned as the world-leading companies of MLCCs, have launched miniature oxide-based ASSBs to the market.[99–102] While their usage is still limited to small electronic devices because the net capacity is low due to their small size, those micro-batteries validate that the cell configuration of stacked thin layers of anode|SE|cathode mimicking that of MLCCs (Fig. 1) is potent to increase the capacity and enhance the rate capability. The overall capacity of an MLCC-type ASSB is the sum of the capacities of all cathode (or anode) layers, while the thinner electrode layer offers a lower intrinsic resistance, resulting in a higher rate capability.

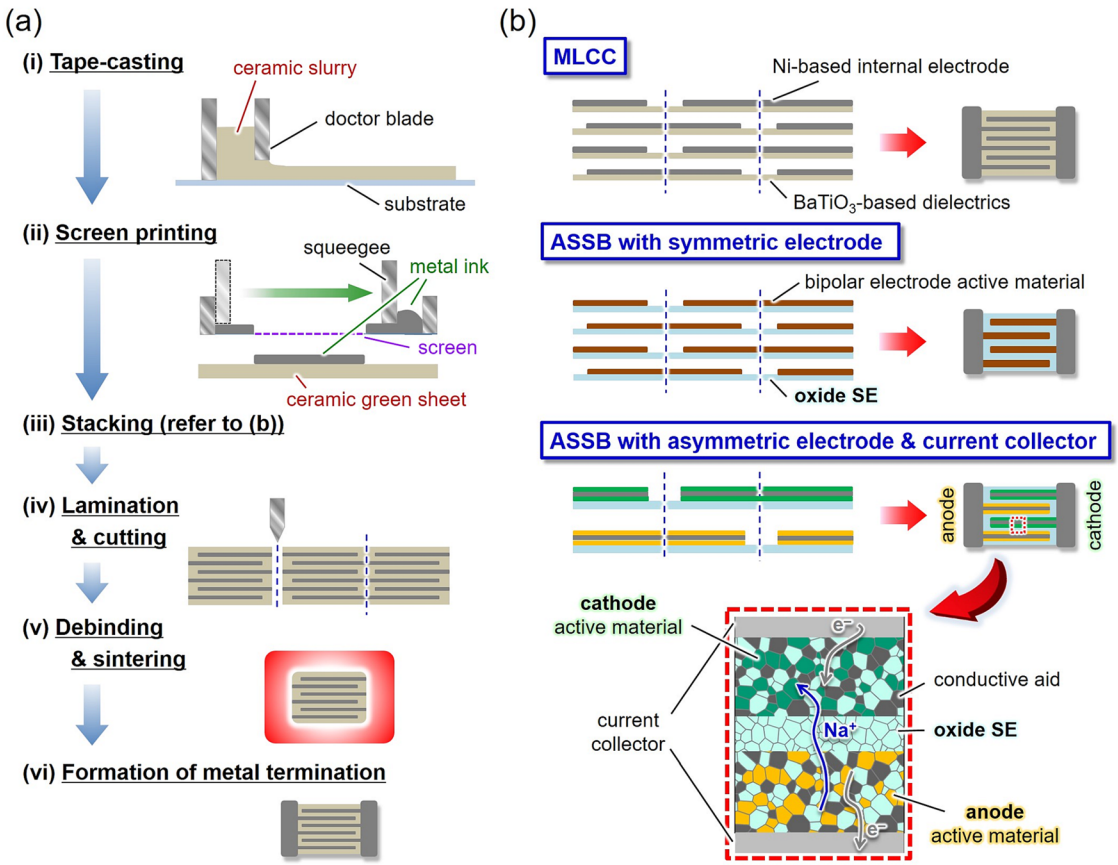

FIG. 1. Manufacturing MLCCs and MLCC-type Na-ASSBs via the tape-casting process: (a) production procedure of MLCCs and the expected production of oxide-based Na-ASSBs that mimic the MLCC-production; (b) ways of stacking for making a typical MLCC and two types of ASSBs. The dotted lines represent the cutting point after lamination. In the ASSB with symmetrical electrodes reminiscent of the MLCC structure, the electrode layer contains single or multiple electrode active material(s) corresponding to the positive and negative electrode reactions, and a conductive aid and an oxide electrolyte may be mixed with each layer. In the ASSB with asymmetric electrodes aiming at enhanced energy density, the electrode active materials corresponding to the positive and negative electrode reactions are applied on an internal current collector layer, respectively.

When it comes to Na-ASSBs, commercialization is yet to be realized, even in miniature size. However, the Na–ion ceramic conductors have a long history and are ahead of their Li–ion counterparts in terms of ionic conductivity despite the larger ionic size since the discovery of outstanding ionic conductivity for Na-β/β''-alumina by Yao and Kummer in 1967,[103] now exceeding 10^{-2} S cm^{-1} at 25 °C.[104–108] The layered crystal structure of Na-β/β''-alumina constituted by Al–O spinel blocks embraces the two-dimensional (2D) spacing called "conduction planes," where Na^+ ions are able to move smoothly. This superionic conductor gave birth to the practical energy storage systems of Na/β''-alumina/S (NAS battery) and Na/β''-alumina/$NiCl_2$ (ZEBRA battery) operated at 270–350 °C, in which a pair of electrodes work in a liquid state.[107,108] Nevertheless, Na-β/β''-alumina necessitates a fairly high sintering temperature (typically ~1600 °C) for adequate densification.[104–108] About a decade later, Goodenough *et al.* designed and elaborated the three-dimensional (3D) polyanion-based framework where Na^+ ions can move fast (10^{-4}–10^{-3} S cm^{-1} at 25 °C), the so-called Na superionic conductor (NASICON).[109,110] Notably, well-sintered SEs of NASICON can be obtained at lower temperatures, like 1100–1250 °C,[109–113] and the sintering temperatures can be further reduced, which is described in detail later. Afterward, multifold compounds with a crystal structure similar to NASICON have come out to date, forming an enormous family of NASICON-type compounds applicable to not only SEs but also electrode active materials.[114–118] Along this line, Na-ASSBs based on NASICON show great promise in view of future industrialization.

In this article, we briefly overview recent research progress on Na-ASSBs based on oxide-based SEs, in particular, NASICON, with an eye on the tape-casting process. Since a broad spectrum of reviews on SEs and ASSBs have been published with frequent updating recently,[26–36,43–45,48,71–73,86] our insights into how to overcome the difficulties in preparing NASICON-based SE films and integrating with cathodes and anodes into Na–ion ASSBs are addressed from a technical aspect in light of the relevant research activities in our group instead of a comprehensive summary in this field. As the production cost projection based on the tape-casting technology is outside the scope of this perspective, interested readers are referred to the seminal literature on this subject.[71,72] Alternatively, the feasibility of a Na metal anode in combination with a NASICON-based SE is discussed according to the studies on interfacial resistance and dendrite growth behavior. In the last section, we provide an outlook on the future direction for designing and manufacturing Na-ASSBs via the tape-casting process toward a practical use.

II. TAPE CASTING

Tape casting,[87–98] also known as the doctor-blade method, is a traditional ceramic process to produce flat films (and thick sheets), yet it still makes progress with emerging new techniques like freeze tape casting to fabricate an exquisite porous structure.[119–123] This technique is currently employed at the forefront of engineering ceramic-based devices including MLCCs, SOFCs, and ASSBs.[91–98,124–134] Ceramic films manufactured by this process are marked by high homogeneity in thickness and microstructure, good controllability of film thickness in the range of 1–1000 μm, large productivity with decent reproducibility (by adopting a flow process), and cost savings. The versatility and applicability to afford a wide range of products, from highly dense films to porous ones, as well as those from single-layer sheets to multi-layer laminates, are also worth highlighting.

Figure 2 illustrates the tape-casting process where a ceramic slurry prepared with a specific composition is cast onto a stationary or moving flat substrate (usually a polymer film typified by Mylar® film), forming a continuous tape with a homogeneous thickness by a so-called doctor blade. After drying under optimal conditions, the green tape is cut or punched into pieces with the desired shape, followed by thermal treatments (debinding and sintering). In practice, there are many matters to be attended to in each process to obtain truly high-quality ceramic films. The most important factors that determine the properties of final products (microstructure, density, thickness, surface flatness, and mechanical strength) are the slurry formulations and processing parameters. As for the former, the ceramic slurry is prepared by mixing ceramic powders of interest with various additives: surfactants to expedite the dispersion of particles (viz., dispersants and deflocculants), binders to adhere particles together, plasticizers to impart flexibility to a green tape and assist in preventing crack formation during drying and handling in the following processes, and solvents as dispersion media.[88–90,125,135–140] Sintering agents are usually added as well, with the intention of obtaining densified ceramics.[141–144] The processing parameters involve the machine configuration, substrate velocity, and blade height and width, which allow for precise control over the physical properties of green tapes and, eventually, final ceramic films because these parameters can be more readily and flexibly varied than the slurry formulation.

The rheology of a slurry depends on the ingredients and their contents and has a large influence on the physical properties of the resultant green tapes and sintered products.[90,140] Hence, it is necessary to carefully optimize the slurry compositions individualized for each material. One should also pay attention to the particle size and distribution of ceramic powders as the main component of a slurry; in general, the finer particle with the narrower size distribution is favorable for better sintering thanks to the shorter diffusion distances and the larger driving force for densification.[144–147] It should be noted that, however, too small a particle size is detrimental to the processability of a slurry because of the lowered dispersibility and increased agglomeration tendency; the favorable particle size normally ranges from submicrons to a few micrometers.[88] Since all the ingredients must be thoroughly mixed together in a homogeneous slurry without any agglomeration, the mixing process should be carried out stepwise: ceramic particles are first dispersed into a solvent using appropriate dispersants, resulting in a low-viscosity suspension, followed by adding other additives such as binders and plasticizers to form a viscous slip. When more than two kinds of ceramic powders are employed (e.g., an electrode active material and an SE), it is essential to make the two particle densities similar in order to preclude inhomogeneous settling between an interval of the two mixing stages. To ensure a complete mixture with high dispersibility, special mixing processes are often leveraged, e.g., planetary mixing and ball milling. As it is inevitable that vigorous mixing of a viscous slurry leaves bubbles, which are hardly dispelled, causing the formation of voids and pinholes, the produced slurry

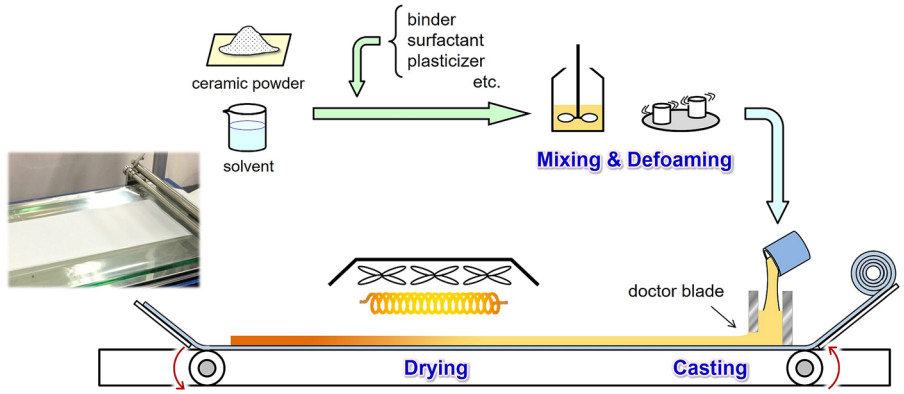

FIG. 2. Overview of the tape-casting process involving (i) mixing, (ii) defoaming, (iii) casting, and (iv) drying. The digital photograph represents a typical ceramic green sheet prepared in a laboratory.

must be subjected to a defoaming process before casting, for example, stirring under vacuum, centrifugation, and ultrasonication. The addition of defoamers or antifoamers is also useful to deter foaming and dissipate bubbles.[148]

Stringent control of slurry viscosity by adjusting the binder content in conjunction with those of the other constituents is crucial for ensuring homogeneity in a green tape: relatively high-density ceramic particles are liable to settle out in a low-viscosity liquid even in the presence of surfactants, whereas an excessive increase in slurry viscosity by adding a lot of binders makes it difficult to pour the slurry onto a substrate and level off with a doctor blade. In order to address this issue, the tape-casting process makes use of pseudoplastic behavior, in which the viscosity of a fluid decreases with increasing shear force and vice versa.[88,90] Specifically, the binder concentration is tuned to render the slurry viscosity high enough to hinder the sedimentation, while the viscosity may decrease by several orders of magnitude upon casting due to the high shear force applied and, soon after the doctor blade passes through, increase again rapidly to keep the homogeneity.[88] As such, the fabrication of a homogeneous tape with a controlled thickness is achieved by moving either a doctor blade or a substrate relative to the other; the latter enables continuous production suitable for industrial manufacturing.

A casted tape is subsequently submitted to a drying step, where volatiles in the tape are evaporated merely from the surface while the liquid diffuses from inside to the surface. A wet tape is exposed to capillary force upon evaporation, leading to internal stress, which fosters densification but simultaneously incurs an inhomogeneous shrinkage that possibly causes crack formation.[149] Hence, the drying process needs to be carefully regulated as well. Usually, gentle heating and blowing are applied so as to keep the drying speed constant. It should be stressed that the proper addition of binders and plasticizers is requisite for preparing a crack-free green tape, as mentioned earlier. In general, thicker tape is more difficult to dry without cracking because of the larger extent of non-uniform shrinkage along the thickness direction.

The next process after drying is shaping, where a large green tape is cut or punched into small pieces with a desired size and shape, as it becomes difficult after thermal processes due to the loss of flexibility and plasticity. As for the preparation of multi-layer ceramic products, the corresponding green tapes removed from support are stacked together and pressed with heat, followed by the cutting process. Thermal compression at a temperature above the softening point of an employed binder/plasticizer system yields coherent multi-layer bodies. There are many routes to making multi-layer ceramic products other than this procedure,[69–72,91–94,150–152] which are beyond the scope of this article.

In the final thermal process, a shaped green body is first degreased by firing in the air at 400–600 °C to pyrolyze all organic species (debinding)[153,154] and then sintered at high temperature to accomplish full densification. Both debinding and sintering processes entail unignorable shrinkage, which imposes cracking, blistering, curling, and crumpling; in contrast to the aforementioned drying step, the thinner film is more delicate, although a film shrinks to a larger extent normal to the thickness than the in-plane direction as in the case of drying.[154–156] Concerning the debinding process, in particular, the decomposition of organic additives results in the volumetric decrease of solid moieties concomitantly with gas evolution, enhancing the internal stress. Accordingly, careful control of the heating conditions (heating rate, temperature, duration time, and atmosphere) is required to maintain the integrity of the final products. In general, a rapid elevation of temperature causes severe damage to a tape sample, as does the cooling,[157] though the short processing time is favorable in terms of a high production rate and low heating energy. Moreover, carbonaceous residues may form through the rapid pyrolysis of organic components upon raising the temperature,[158] which often deteriorates the relatively low density of a sintered body, leaving many pores.[159] Another practical matter is the adhesion of a ceramic film to a platform in a furnace during thermal treatment, which sets off cracking and fracturing. Specific ceramic setters with some coating and/or a scabrous surface can remedy this issue. In addition, when sintering of a targeted material requires high temperatures where evaporation of volatile elements unignorably occurs, specimens need to be buried in mother powder on firing (i.e., buried powder sintering or burying sintering) in order to suppress the volatilization and

consequent decomposition. For the sake of enhancing the relative density of a sintered film, the hot pressing technique is used in the final sintering process.[160–164]

Practically, all of the variable parameters in the tape-casting process described earlier are modulated in an empirical manner, depending on the types of ceramic films in view of materials and structures for satisfying the criteria of intended use. Furthermore, since the optimal condition differs according to the production location due to the difference in facilities and ambient environment, temperature, and humidity, the adequate synthetic conditions need to be deciphered based on a fund of experimental data collected with an individual manufacturing setting pertaining to the correlation between the processing parameters (viz., the composition of slurry associated with its rheology, blade height, moving velocity, etc.), the manipulation ways (for mixing, casting, shaping, drying, and thermal treatment), and the nature of the final products including thickness, relative density, microstructure, crystallinity, and so forth. All these properties are entangled with ionic conductivity as far as SE films are concerned.[125–134] In addition, from an industrial point of view, one should also pay attention to other matters of product quality, yield ratio, and reproducibility, all of which are closely linked to production cost.

III. PROPERTIES OF NASICON ELECTROLYTES DEPENDING ON SINTERING PROCESS

As a critical component of ASSBs, several requisites should be fulfilled to be a potent oxide-based SE: (i) high ionic conductivity comparable to those of liquid electrolytes together with an electronically insulating feature to act as a separator that prevents current leakage and self-discharge during an idle period; (ii) a wide electrochemical stability window enough to afford high voltage; (iii) large-scale producibility with the use of earth-abundant and environmentally benign materials; (iv) good processability (preferably in the air) and sinterability at a reasonable temperature so that unfavorable volatilization of Na and other easily volatile elements does not severely take place. As pointed out previously, the old-established Na–ion conductor, NASICON,[109–118] satisfies these criteria except for the last point. In addition, the continuous efforts in the ceramic engineering field have borne fruit with the technical advances in the fabrication of well-sintered and high-quality NASICON at lowered temperatures, such as flash sintering,[165] microwave sintering,[166] spark plasma sintering (SPS),[167–170] and cold sintering.[170–172] Note that to integrate an SE with a pair of electrodes into ASSBs, the capability of establishing intimate interfaces between the SE and electrodes with a large area as well as their mechanical and structural stability during the repeated charge and discharge operation are of decisive importance, and precisely these points are connected to the most formidable challenges, especially in the case of oxide-based SEs, which is discussed not in this section but later on.

NASICON originally stood for the solid solution between $NaZr_2(PO_4)_3$ and $Na_4Zr_2(SiO_4)_3$ endmembers, expressed as a general formula $Na_{1+x}Zr_2Si_xP_{3-x}O_{12}$ ($0 \le x \le 3$).[109,110] The NASICON crystal structure is built up of corner-sharing ZrO_6 octahedra and $(Si,P)O_4$ tetrahedra forming the 3D rigid framework composed of a unique structural unit called "lantern," which provides the large interstitial channel for Na^+-diffusion. It allows for the fast 3D migration of Na^+ ions, which is advantageous over the 2D ionic conductor like Na-β/β''-alumina when it comes to polycrystalline SEs because the random orientation of crystallites in an SE layer diminishes the overall conductivity suffering from the contribution from grains residing in poorly conductive directions.[106] As elucidated in the first publication of NASCION,[109] the NASICON solid solution exhibits the highest conductivity with the composition of $Na_3Zr_2Si_2PO_{12}$ ($x = 2$), which is denoted as "NZSP" in this article. Here, we mainly deal with the simple NZSP in conjunction with the tape-casting process, as the NASICON family involves plenty of substitutional variants.[112,113]

Given that the standard interspacing distance between two electrodes in conventional LIBs with a liquid electrolyte is 20–30 μm, which corresponds to the thickness of a polymer separator such as Celgard®,[173] the thickness of a NASICON layer is desired to be less than 100 μm in ASSBs so that the resistance within the SE layer is on par with that in LIBs. In this sense, the tape-casting process is suitable to fabricate NASICON films for ASSBs. Meanwhile, because the grain boundary resistance (R_{gb}) is generally orders of magnitude higher than the bulk resistance (R_{bulk}) and, therefore, dominant in the resistivity of an electrolyte layer, the densification of SEs for increasing the interparticle contact area and growing the grain size to the maximum extent is imperative to ASSBs. However, it becomes more difficult to obtain well-sintered ceramics at low temperatures by means of the pressureless process in comparison with the dedicated sintering procedures relying on mechanical pressure and/or electric current.[174–179]

The addition of sintering aids (or fillers),[144] which was first discovered in sintering Al_2O_3 promoted by a small amount of MgO,[141] is well-known as a complementary technique to densify ceramics available for any sintering process, including tape-casting. Such additives offer an economic advantage in the production of sintered ceramics by shortening the process time and decreasing the sintering temperature. There are several mechanisms proposed for the enhancement of sintering in dependence on the kinds of additives, some of which are still controversial.[142,144] Sintering assisted by a liquid phase is a major consolidation phenomenon in powder compacts, and most sintering aids, such as compounds with a low melting point, play a role in the liquid phase at elevated temperatures. Reagents that decrease the melting point of a target are conducive to liquid-phase sintering as well. This sintering system consists of three processes: (i) rearrangement of solid particles with the help of a flow of melt driven by capillary pressure; (ii) progress of densification by dissolution and reprecipitation of the solid in the formed liquid; and (iii) relatively slow densification by coalescence between solid grains that are not wetted.[142,144] The liquid phase either depletes during sintering or remains until the last stage. In the former case, elements in sintering aids are to be more or less introduced into the crystal lattice, whereas segregation of additives at the grain boundary occurs in the latter.

Sintering agents employed for SEs should not disturb the aforementioned requisites, particularly electrochemical properties (conductivity and stability). The segregated phase derived from sintering agents at the grain boundary usually spoils the total conductivity of an SE by acting as a barrier against ionic transport, though the grain-boundary conduction is, by contrast, enhanced with additives in some cases.[180–187] Electrochemical stability is often deteriorated

TABLE I. Sinterability and electrical conductivity of the NZSP SEs sintered with different sintering agents.

Sintering agent	Melting point (°C)	Sintering method	Content (wt. %)	Sintering temperature (°C)	Relative density (%)	$\sigma_{25\,°C}$[a] (S cm^{-1})	Reference
NNP glass[b]	730	SPS[c]	5	1045	98	1.0×10^{-3}	168
		CS	10	900	···	1.2×10^{-4}	189
Na_3BO_3	680	CS	4.8	900	93	1.4×10^{-3}	192
		CS	9.1	700	73	1.2×10^{-4}	193
$Na_2B_4O_7$	741	SPS[d]	10	600	82	2.3×10^{-4}	169
		CS	10	1000	···	1.72×10^{-3}	196
Na_2SiO_3	1088	CS	5	1175	93	1.45×10^{-3}	195
$Na_2Si_2O_5$	848	CS	5	1150	77	1.7×10^{-3} [e]	198

[a]Total conductivity at 25 °C.
[b]$60Na_2O–10Nb_2O_5–30P_2O_5$ glass.
[c]Spark plasma sintering at 50 MPa under vacuum.
[d]Spark plasma sintering of Mg-NZSP [$Na_{3.1}Zr_{1.95}Mg_{0.05}(SiO_4)_2(PO_4)$] at 102 MPa.
[e]Measured at 27 °C.

by contaminated elements, as the integrity of the crystal lattice is bound to be disturbed. In addition, the atoms with variable valency are liable to redox reactions, which are responsible for the decomposition of an SE. Hence, a compound consisting of main-group light elements and/or sharing components of a target SE is favorably employed as a sintering aid.

In the case of NASICON-based SEs, several sintering aids have been investigated in conjunction with the different sintering techniques,[168–170,172,188–198] which are summarized in Table I. For instance, the addition of borax ($Na_2B_4O_7{\cdot}10H_2O$) allows for the densification of NZSP to possess ~10^{-3} S cm^{-1} of room-temperature total conductivity at as low as 600 °C by SPS.[177] The newly developed cold sintering technology is also capable of producing a highly conductive NZSP SE in combination with post-annealing and adding NaOH as an aid, although cold sintering alone fails to increase the total conductivity of NZSP to a practical level.[170,172] Regarding ambient-pressure sintering, Na_3BO_3 effectively promotes the sintering of NZSP, yielding a high-density compact (relative density of ~93%) at 900 °C.[192,193] Nevertheless, these compounds are soluble in water and aprotic organic solvents to form a basic solution, which is possibly detrimental to ingredients in the tape-casting process.

Another option for sintering aids is glass additives.[188–190,197,198] Among them, the $Na_2O–Nb_2O_5–P_2O_5$ (NNP) glass exemplifies an effective filler for sintering NZSP.[189,190] The alkali niobate glass shows relatively high Na–ion conductivity around room temperature and low glass transition temperature (T_g) and melting temperature (T_m) among the oxide-based glass.[189,199–201] Despite the variable valency of Nb, the stable pentavalent state (Nb^{5+}) guarantees a wide electrochemical stability window by forming an interfacial passivation film.[202–204] In the NNP system, the composition $60Na_2O–10Nb_2O_5–30P_2O_5$ has a high conductivity (2.6×10^{-7} S cm^{-1} at 25 °C) as well as a low melting point of ~730 °C, as presented in Fig. 3.[168] Accordingly, the NNP glass is eligible for the sintering aid of NZSP films prepared via the tape-casting process.

The capability of NNP glass additive in sintering NZSP green tapes is signified in Fig. 4(a), in which the NZSP sintered disks are compared as a function of the amounts of NNP glass additive and sintering temperature.[190] The disks started with the green sheets, which were almost identical in terms of dimension (15 mm in diameter and 45–50 μm in thickness) and composition (binder, plasticizer, dispersant, and defoamer) except for the NNP glass content. The additive-free NZSP green sheet experienced limited shrinkage up to 1100 °C, and the thermal treatment at 1230 °C for 4 h encompassed crumpling as the densification proceeded. It transpired that the high sintering temperature prompted the volatilization of Na and P from NZSP, which imposed heterogeneous shrinkage, thereby resulting in the wrinkled film. This result clarifies the difficulty of producing a sintered NZSP film without sintering aids. On the other hand, the disk diameter obviously diminishes as the NNP content increases for the samples heated above 1000 °C, which validates that the NNP glass effectively stimulates the sintering of NZSP, probably through the liquid-phase sintering mechanism. As a result, the 5 and 10 wt. %-NNP added samples sintered at 1100 °C appear to be translucent, indicating the depletion of pores, which is also attested by the microstructural images shown in Fig. 4(b).

The sinterability of NZSP films aided by the addition of NNP glass was further evaluated from the standpoint of gas permeability [Figs. 4(c)–4(e)].[190] The poorly sintered samples provided in Fig. 4(c) showed rapid or gradual gas leakage across the film, whereas the negligible pressure change displayed in Fig. 4(d) ascertains that those samples were highly gastight films with the permeability value below 1.0×10^{-9} m^3 s^{-1}, which corroborates the successful preparation of highly densified NZSP films via the tape casting process with the NNP glass aid. Such a superb impermeability feature opens up the possibility for the NZSP films to be implemented in different types of next-generation rechargeable batteries such as a metal–air battery that requires a liquid-tight SE.[8,205,206]

The total conductivities (bulk and grain boundary) of a series of NZSP sinters prepared via the conventional solid-state (CS) reaction, SPS, and tape-casting with varied amounts of NNP glass are compared in Figs. 5(a) and 5(b). Without any additives, the NZSP SEs showed total conductivities (at 25 °C) of 1.2×10^{-3} S cm^{-1} (CS; 1270 °C for 12 h), 1.7×10^{-3} S cm^{-1} (SPS; 1210 °C for 30 min), and

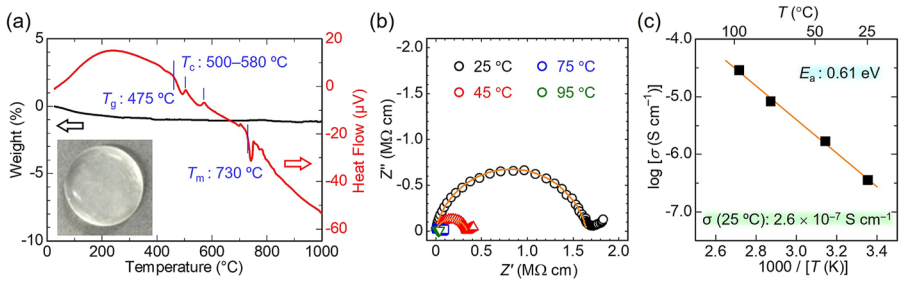

FIG. 3. Physical and electric properties of the NNP glass ($60Na_2O$–$10Nb_2O_5$–$30P_2O_5$): (a) thermogravimetric (TG) and differential thermal analysis (DTA) curves and the colorless and transparent appearance of the NNP glass (inset); (b) impedance spectra of the NNP glass measured at varied temperatures; (c) Arrhenius plot of the NNP glass. Reproduced with permission from Wang *et al.*, Solid State Ionics **322**, 54 (2018). Copyright 2018 Elsevier.

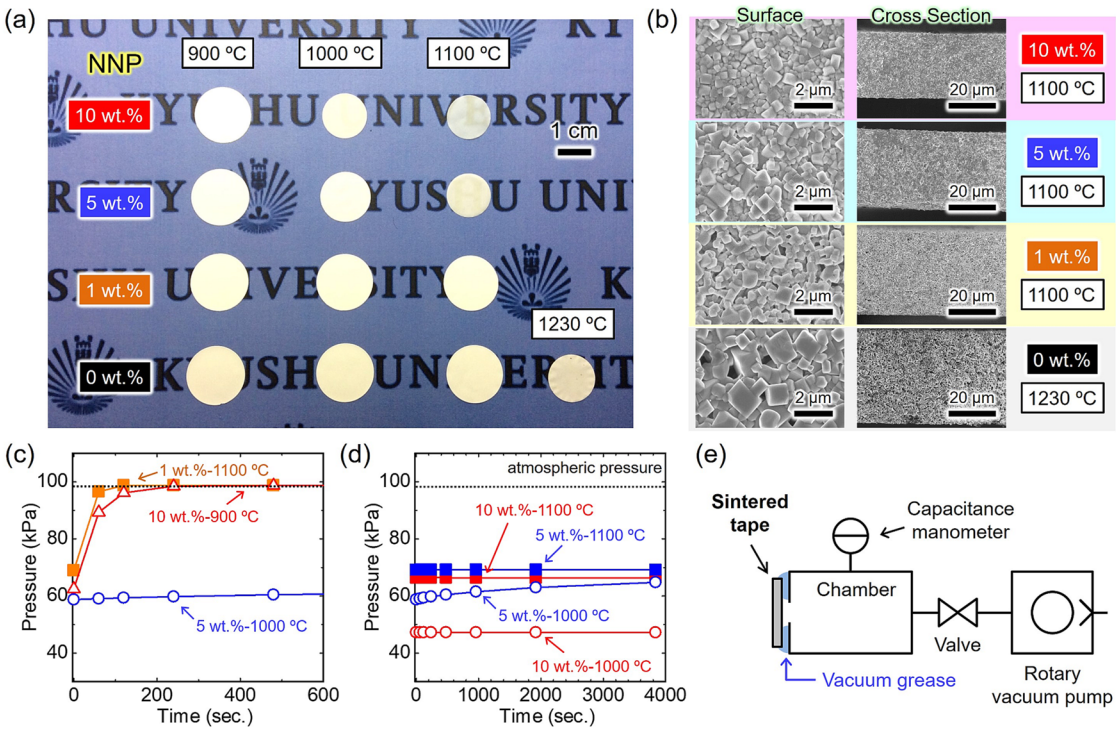

FIG. 4. Comparison of the NZSP SEs prepared via tape casting with the NNP glass additive: (a) appearances of the NZSP disks sintered with different conditions; (b) microstructural morphologies of the surface and cross section of each NZSP sintered disk; (c) and (d) time-dependent pressure change measured with the gas permeability test system in (e) for the respective NZSP sintered disks; (e) schematic illustration of the gas permeability test equipment. Reproduced with permission from Okubo *et al.*, Electrochim. Acta **278**, 176 (2018). Copyright 2018 Elsevier.

3.1×10^{-4} S cm^{-1} (tape-casting; 1230 °C for 4 h).[168,190] The NNP glass additive lowered the sintering temperature of NZSP in each synthetic system, offering those of 1.2×10^{-4} S cm^{-1} (CS; 900 °C for 10 min),[189] 7.2×10^{-4} S cm^{-1} (SPS; 990 °C for 30 min),[168] and 4.4×10^{-4} S cm^{-1} (tape-casting; 1100 °C for 4 h).[190] In all cases, the activation energy for ionic conduction lay between 0.28 and 0.34 eV, as presented in Fig. 5(b). Consequently, the addition of NNP glass can reduce the sintering temperature of NZSP SEs by ~130 °C even in the case of the tape-casting process, while it becomes more effective in combination with CS and SPS techniques. It was also confirmed that the depression of ionic conductivity by contaminating impurities (NNP and its derivatives) is limited in all cases.

The compositional analyses testified to the good quality of the NZSP sintered with NNP glass. Figure 6 shows the XRD profile and elemental mapping images of the representative NZSP specimen (tape-casting; 10 wt. % NNP; 1100 °C).[190] Whatever the synthetic process is (CS, SPS, or tape-casting), the heat-treatment at >900 °C forms the perovskite-type $NaNbO_3$ as a by-product, which is a

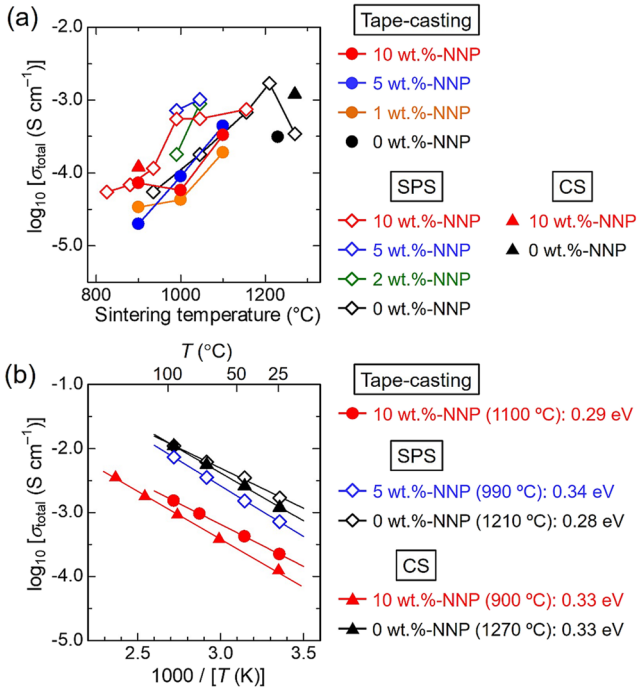

FIG. 5. Ionic conductivities of the NZSP SEs prepared by different sintering procedures [tape casting, spark plasma sintering (SPS), and conventional solid-state synthesis (CS)] using the NNP glass as a sintered agent: (a) total conductivities as a function of sintering temperature; (b) Arrhenius plots of the total conductivities for the representative NZSP sintered SEs.[169,189,190] The activation energy values are based on the relationship between ln σT and $1/T$.

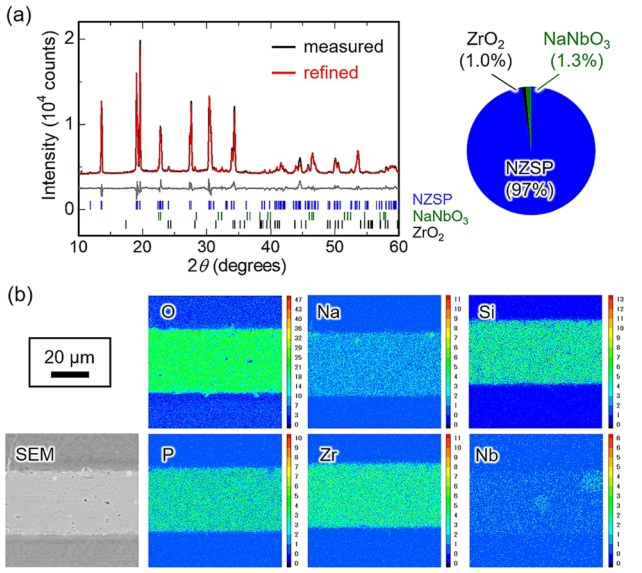

FIG. 6. Compositional characteristics of the NZSP SE prepared via tape casting with 10 wt. % NNP glass sintered at 1100 °C: (a) XRD profile and the composition estimated by Rietveld refinement; (b) electron probe microanalysis (EPMA) images.

poor Na–ion conductor (<10^{-6} S cm^{-1} at 300 °C),[207–209] in addition to the small amount of ZrO_2, which is routinely formed in preparing NZSP.[111,210] In the case of the NZSP film prepared by tape casting, Nb was found to be uniformly distributed without forming large $NaNbO_3$ crystals [see Fig. 6(b)], and hence, the incorporation of Nb into NZSP may have occurred. As for the sample prepared by SPS, on the other hand, the segregation of $NaNbO_3$ grains (~5 μm) was observed in triple junctions of grain boundaries.[168] In both cases, the Na–ion conduction pathway was not crucially perturbed by the incorporation of Nb and/or the contamination of $NaNbO_3$, as manifested by the good ionic conductivity and low activation energy in Fig. 5. A wide electrochemical stability window for these NZSP SEs was documented by the experimental results with the corresponding Na|NZSP|Pt cell demonstrating reversible Na plating/stripping and negligible anodic current up to at least 4.1 V.[168]

IV. NASICON-TYPE CATHODES FOR TAPE CASTING

As is the case with LIBs, multifold cathode materials for SIBs have been developed along with a liquid electrolyte,[20–25] yet all of them are not necessarily applicable to Na-ASSBs. In other words, a cathode candidate for Na-ASSBs needs to satisfy more stringent requirements. Whether the electrolyte is liquid or solid, the electrode layer must be a mixed electron–ion conductor to carry electrons to the current collector and Na^+ ions to the electrolyte. Nonetheless, most electrode active materials do not possess electronic and ionic conductivity high enough for practical usage. Therefore, carbon-coating on particle surfaces and the addition of conductive agents are usually implemented to ameliorate the electronic conductivity, which is also applicable to ASSBs. Meanwhile, the general strategy to address the low ionic conductivity issue is to diminish particle size to minimize ionic conduction pathways in solids. It works out well in conventional LIBs as ions migrate predominantly in a liquid electrolyte, which percolates throughout the electrode layer wetting all the particle surfaces. As for the ASSB configuration, particularly with a stiff oxide-based SE, however, this approach is far less effective. This is because of the difficulty in establishing a perfect contact between the active material and SE particles simultaneously with the interconnectivity of all SE components to offer 3D ion-conducting pathways, and what is more, the mandatory thermal treatment at high temperature entails crystal growth, making it hard to preserve small particle size in ASSBs.[27–33]

Incorporation of an electrode active material mixed with a conductive agent into a 3D porous scaffold consisting of an SE seems like a smart methodology to produce a cathode layer. The addition of sacrificial pore-forming agents (also called porogens) such as organic molecules (carbohydrates like starch and polymer beads) and carbonaceous species (graphite and amorphous carbons) to a ceramic slurry is a simple way to intentionally introduce pores in ceramic sheets prepared via tape casting.[123,211,212] These additives burn away during firing and sintering, leaving pores and voids in the final ceramic sheet. As a more advanced methodology to control pore properties, the freeze-tape-cast technique was developed as well.[119–123] However, it is generally difficult to tailor exquisite 3D scaffolds using powder-based ceramic processing, unlike solution

processes such as sol–gel, which can produce porous materials with controlled pore properties in conjunction with self-assembly,[213,214] colloidal templating,[215] and phase separation.[216–218] On this account, a cathode candidate for Na-ASSBs should have moderate ionic conductivity, if not as high as that of SEs.

Another criterion for choosing an electrode material for ASSBs is its structural stability during charge and discharge cycles,[75–78] which is associated with cyclic performance and longevity. ASSBs are sensitive to internal stress arising from the volume expansion/shrinkage of electrode materials because the scarcely deformable SE can tolerate only a little volumetric change, in stark contrast to a liquid electrolyte. Consequently, even once a coherent interface was successfully prepared, it remains a daunting challenge to maintain intimate solid/solid contact through long-term cycling. Hence, potential electrode materials fall into the "rocking-chair" type of electrode, consisting of a rigid framework that allows for a nearly "zero-strain" insertion/extraction reaction.[219–236] Smooth Na–ion transfer at an electrode/electrolyte interface is of great significance to achieving high power density, though there have been a small number of studies on this subject thus far. In addition, it is indisputable that a cathode with higher capacity and higher operational potential leads to higher energy density, which is favorable for a practical cell.

In view of good ionic conductivity and a small crystallographic volume change upon sodiation/desodiation, some specific layered oxides,[224–228] Prussian blue analogs (PBAs),[229–234] and polyanion-type compounds[235,236] have been reported as highly promising SIB cathode materials. The layered oxide-type SIB cathodes are represented by Na_xCoO_2, which is a forerunner material first reported in 1980.[237] Although the layered oxides generally undergo a large volume change in concert with the crystal transition, several zero-strain electrode candidates have recently emerged from the elaborate crystallographic design with cation substitutions.[222–228] The preceding studies on Na-ASSBs in tandem with the layered oxides were limited to Na_xCoO_2, where the layered oxide thin film was directly deposited on an SE by means of pulsed laser deposition (PLD).[238,239] The PBAs $\{A_xM_y[M'(CN)_6]_z$, where A is an alkaline metal while M and M' are transition metals$\}$ are featured with their open framework crystal structure, thereby enabling reversible ion storage/release with a minimum volume change.[229–234] The low-cost and scalable solution process at room temperature for PBA production makes them the top contender for a cathode for launching practical SIBs with a liquid electrolyte. Nonetheless, the low thermal stability of PBAs seems to be incompatible with oxide-based SEs that require high-temperature sintering.

Among the polyanion-type compounds, the NASICON-type cathode materials have a high potential in terms of their robust crystal lattice with 3D continuous ion-conducting channels.[115–118] This category of crystals has the formula $A_xM_2(XO_4)_3$ or $A_xMM'(XO_4)_3$, where A = Li, Na, K, etc.; M/M' = Al, Cr, Mn, Fe, Ti, Zr, V, Nb, etc.; and X = P, Si, S, etc.,[115–118] and is a distinctive feature of the 3D covalent framework composed of fully corner-sharing $M(M')O_6$ octahedra and XO_4 tetrahedra in analogy with NZSP.[109,110] When transition metals for M and M' are electrochemically redox-active to permit the variation of A-ion occupancy in a wide range, the NASICON-type crystals are capable of being electrode active materials for rechargeable batteries. There is a large interstitial space inside the robust 3D framework where alkali metal ions (A^+ ions) reside. In general, the NASICON-type compounds fall into either rhombohedral ($R\bar{3}c$) or monoclinic phase ($C2/c$ or Cc); the former embraces three crystallographic sites for A^+ ions (Wyckoff positions of 6b, 18e, and 36f), while site splitting due to lattice distortion takes place for the respective sites in the latter.[118] Accordingly, the NASICON-type compounds are expected to procure decent ionic conductivity due to the pronounced 3D channel for ion diffusion and the presence of vacant sites. If the target electrode active material has adequately high ionic conductivity, the requisite amount of SE contained in an electrode layer to enable the feasible operation of ASSBs can be drastically reduced or even zero. In addition, the robust 3D framework can mitigate volumetric change upon insertion/extraction of A^+ ions, even when the occupation number largely varies. By virtue of these features, the NASICON-type electrodes tend to undergo charge and discharge in the fashion of a two-phase reaction giving rise to a well-defined potential plateau,[115–118] which is beneficial for delivering a stable voltage when implemented in a full cell.

Recently, in addition to the cation-substituted members,[116,118] the anion-substituted compounds (so-called mixed-anion materials[240]), such as mixed phosphates $[Na_4M_3(PO_4)_2(P_2O_7)$[42,241–244] and $Na_7M_4(P_2O_7)_4(PO_4)$[245,246]], fluorophosphates $[Na_3M_2(PO_4)_2F_3]$[247–249]/oxyfluorophosphates $[Na_3(MO_{1-x}PO_4)_2F_{1+2x}]$,[250–252] nitridophosphates $[Na_3M(PO_3)_3N]$[235,236] and so on,[115,117,253–255] have been developed, which participate in the group of NASICON derivatives in a broad sense (as their crystal structures are somewhat altered from the original NASICON-type structure). The substituted NASICON derivatives provide various merits like the augmented operational potential and the reduced volume change during Na^+-insertion/extraction, which lead to the enhancement of cell voltage and the improvement of cycle performance, respectively. However, the more complicated chemical composition makes phase control more difficult, even for samples in a powdery state, let alone in a sintered layer. Hence, the following puts a focus only on the simple NASICON-type electrode materials.

After the pioneering work demonstrating the electrochemical alkali ion insertion/extraction behaviors of $ATi_2(PO_4)_3$ (A = Li and Na) by Delmas *et al.*,[256,257] the NASICON-type compounds have been recognized as a leading cathode candidate from the standpoint of high rate capability as well as salient cycle performance.[115–118,253–255] Behind the Ti-based NASICON-type compounds, the V-based analog of $A_3V_2(PO_4)_3$ (A = Li and Na) emerged as a superior cathode material because of the higher potential of the V^{4+}/V^{3+} redox couple (~3.4 V vs Na^+/Na) compared to that of Ti^{4+}/Ti^{3+} in $NaTi_2(PO_4)_3$ (~2.1 V vs Na^+/Na).[258–262] Thereupon, various advantageous aspects of $Na_3V_2(PO_4)_3$ (NVP) as a SIB cathode have been realized not only with a liquid electrolyte[261–264] but also in ASSB configurations.[265–272] Although the theoretical capacity is not markedly high (117.6 mAh g^{-1} for the V^{4+}/V^{3+} redox couple), NVP shows high stability in the air, flat charge/discharge curves with small polarization, and good cycle performance. Notably, the two-phase reaction between NVP and $NaV_2(PO_4)_3$ corresponds to a volume change of only 8%–10%,[262–264] which is as small as that of $LiFePO_4$, renowned for a small volume change cathode for LIBs.[273,274] Within the range of such a low volume change, a small amount of porosity persisting in an electrode layer can poise a whole monolithic cell against inner stress.[275,276] Consequently, the NASICON-type NVP is identi-

fied as an ideal cathode for Na-ASSBs, and indeed, some prototype Na-ASSBs have been developed by different research groups in the last decade.[265–272] Along this line, our contribution to the tape-casting technology to obtain a sintered NVP electrode layer is introduced hereinafter.

In a bid to develop a serial processing to produce ASSB laminates involving tape-casting, stacking, and co-firing, we have explored the synthesis of NVP films via the tape-casting process with the aid of the NNP glass additive[277] in a manner analogous to the NZSP films described previously.[190] Figure 7(a) displays a series of NVP green tapes and films sintered with varied amounts of NNP glass at different sintering temperatures.[277] As is the case with the NZSP system in Fig. 4(a), the NVP green tapes were punched out to be a disk with 15 mm in diameter and 40–50 μm in thickness by adjusting the tape-casting parameters. The additive-free and 2 wt. % NNP-containing NVP samples resulted in a similar final disk size after heating at 880–1000 °C, whereas the NVP disks were subjected to discernible shrinkage by the thermal treatment. By contrast to the NZSP case, the addition of 10 wt. % NNP glass caused fatal fracturing in the NVP system. The microstructural observation [Fig. 7(b)] and gas permeability test results [Fig. 7(c)] corroborate that the NNP glass can sufficiently promote the densification of NVP to reach the gas-tight level: 6.8×10^{-9} m^3 s^{-1} for the sample containing 5 wt. % of NNP and sintered at 920 °C.

The well-sintered NVP disk allowed us to properly measure the electrical property of NVP [Figs. 7(d) and 7(e)], providing reliable ionic conductivity values: the bulk conductivity of NVP was estimated as 6.5×10^{-5} S cm^{-1} at 25 °C and 3.2×10^{-4} S cm^{-1} at 90 °C.[277] As the electronic conductivity measured by the direct current (DC) polarization was in the order of 10^{-9} S cm^{-1} at 25 °C, as plotted in Fig. 7(e), the total Na–ion conductivity of the NVP sheet proved to be considerably high among the SIB electrode materials. Consequently, NVP is endowed with adequately high ionic conductivity in association with the small volume change during Na^+-insertion/extraction and, therefore, is regarded as a viable cathode choice for Na-ASSBs.

Differently from the NZSP sinters with NNP glass additive, the XRD analysis revealed that the $NaNbO_3$ perovskite phase was not formed while the unidentified peak appeared with 5 wt. % of NNP glass in the NVP system [Fig. 8(a)]. The high-resolution electron transmission microscopy (HR-TEM) accompanied by elemental analysis in Figs. 8(b) and 8(c) documented the formation

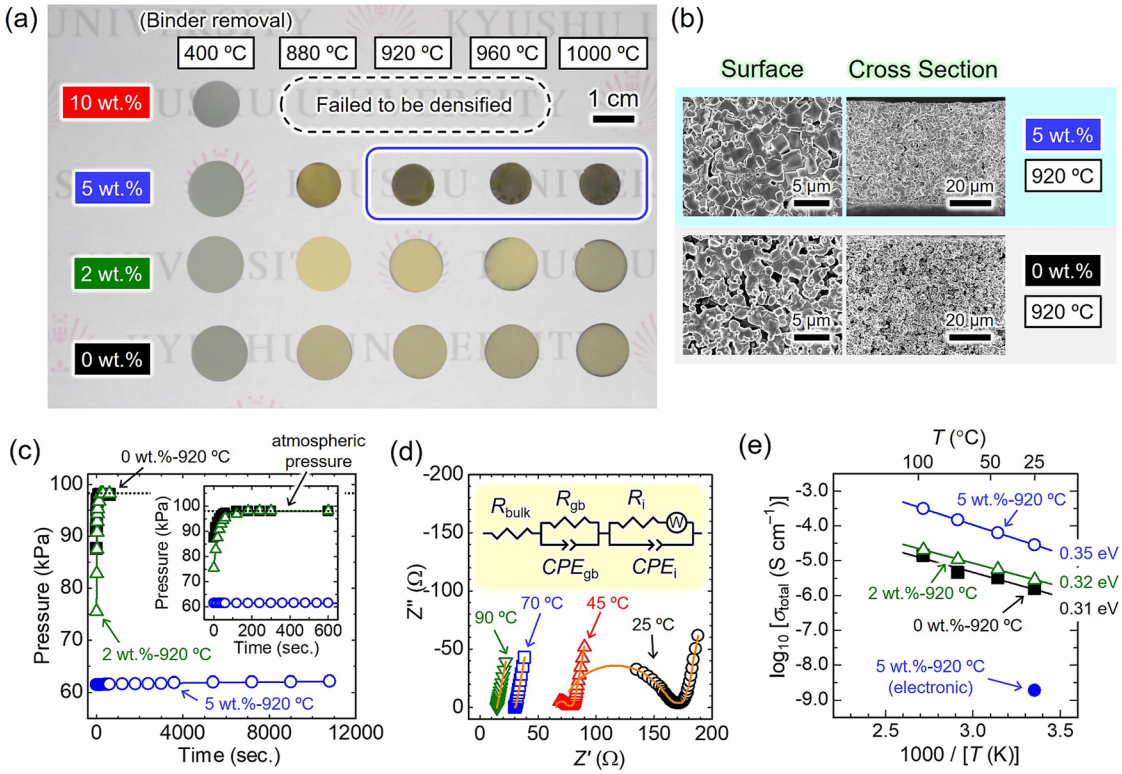

FIG. 7. Comparison of the NVP sintered disks prepared via tape casting with the NNP glass additive: (a) appearances of the NVP disks sintered with different conditions; (b) microstructural morphologies of the surface and cross section for the NVP disks prepared with and without the NNP glass; (c) time-dependent pressure change measured with the gas permeability test system in Fig. 4(e) for the NVP disks; (d) Nyquist plots of the NVP disk (5 wt. % NNP; 920 °C) measured at different temperatures; (e) Arrhenius plots of the total conductivities for the NVP disks prepared with varied amounts of the NNP glass additive. The activation energy values are based on the relationship between ln σT and $1/T$, while the electronic conductivity value is derived from the DC polarization analysis. Reproduced with permission from Wang *et al.*, Electrochim. Acta **305**, 197 (2019). Copyright 2019 Elsevier.

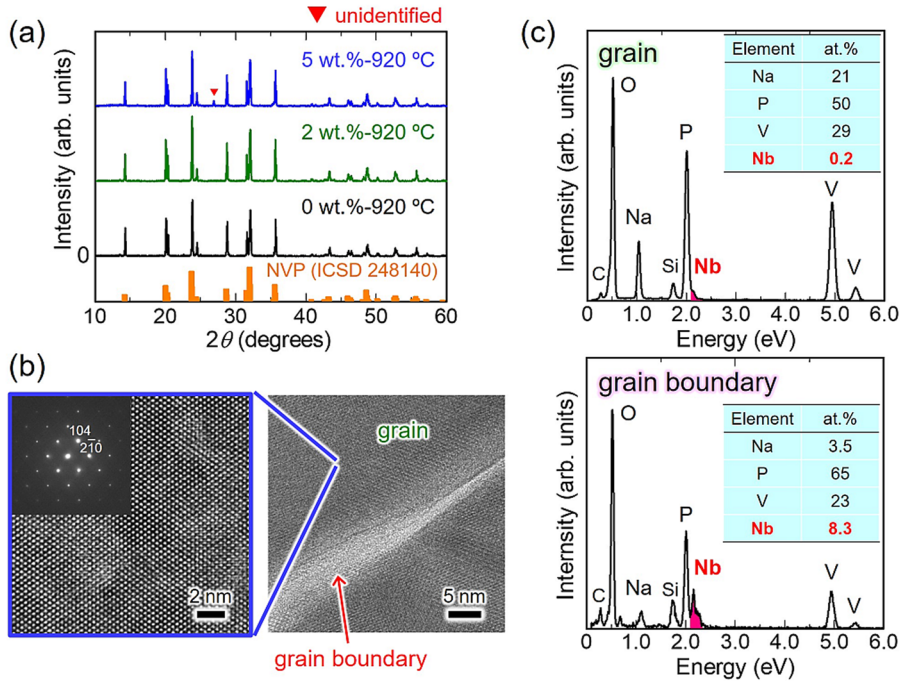

FIG. 8. Chemical compositional and microstructural properties of the NVP disks: (a) XRD profiles of the NVP disks prepared with varied amounts of the NNP glass; (b) HR-TEM images and the selected area electron diffraction (SAED) pattern (inset) of the NVP disk (5 wt. % NNP; 920 °C); (c) energy dispersive X-ray spectroscopy (EDS) analysis results measured in the grain and at the grain boundary of (b). Reproduced with permission from Wang *et al.*, Electrochim. Acta **305**, 197 (2019). Copyright 2019 Elsevier.

of Nb-enriched amorphous moieties at the grain boundaries of NVP crystallites in the NVP film (5 wt. % of NNP and sintered at 920 °C). Nevertheless, according to Fig. 7(d), the grain boundary conductivity of the correspondent specimen was calculated as 5.1×10^{-5} S cm^{-1} at 25 °C, which is compared favorably with that of bulk conductivity. In addition, the activation energy for Na–ion migration in NVP based on the total conductivity [Fig. 7(e)] is in the range of 0.31–0.35 eV.[277,278] Hence, it can be concluded that the NNP glass serves as a good sintering agent for NVP, like NZSP. Furthermore, it is expected that the tape-casting strategy is not limited to NVP but applicable to other electrode materials either as a single component or as a mixture with an SE, though optimization and modification of each synthetic step are indispensable based on empirical trial-and-error processes. Precautions for integrating electrode materials with an SE will be discussed later.

The good ionic conductivity along with the Na^+-insertion/extraction capabilities of NVP allow a well-sintered NVP film to function as a single-component ASSB.[279,280] The single-phase configuration, where the regions in the vicinity of current collectors at both ends act as an anode and cathode while the intermediate region acts as SE, is free from the predominant obstacle of ASSBs: the establishment of innate electrode/SE interfaces. The first proof-of-concept for this type of ASSB was demonstrated concerning a lithium superionic conductor (LISICON), $Li_{10}GeP_2S_{12}$ (LGPS), by Han *et al.* in 2015.[279] They fabricated the LGPS-carbon|LGPS|LGPS-carbon cell (in this regard, this cell contained two components of LGPS and carbon though), in which the LGPS-carbon layers were electronically and ionically conductive and thereby capable of electrodes. When applying a direct current, the Li–S and Ge–S components worked as electroactive species at the positive and negative sides in ways reminiscent of Li_2S and GeS_2, respectively.[279] Inoishi *et al.* reported single-phase Na-ASSBs composed of the NASICON-type $Na_{3-x}V_{2-x}Zr_x(PO_4)_3$ (x = 0–1.0).[280] It was revealed that the 1.1 mm-thick cells delivered ~1.8 V even without carbon additives. However, the relatively large thickness needed to suppress the electron leakage (self-discharge) imposed a high cell resistance,[280] whereas the thinner cell was plagued by the higher self-discharge rate.[277] Nevertheless, since the cell configuration with only one ceramic layer playing three roles (anode, cathode, and electrolyte) can considerably reduce the production cost and be applicable to the MLCC-type structure simply by alternately stacking the ceramic and current-collecting layers, continuous research progress is highly desired.

V. Na METAL ANODE AND OTHER CANDIDATES

Needless to say, the best choice for anode material in Na-ASSBs is Na metal from the viewpoint of energy density because, among all anode candidates, it has the highest theoretical capacity of 1166 mAh g^{-1} and 1129 mAh cm^{-3} and enables the cell to

deliver the highest voltage when the cell is assembled with an identical cathode.[22,281] However, when it comes to the integration with SEs of NZSP and its derivatives, the Na metal anode has long suffered from a remarkably large interfacial charge transfer resistance upon Na-plating/stripping reactions.[282] So far, only the molten Na-based anode in NAS and ZEBRA batteries with the Na-β/β''-alumina SE, in which the operation at elevated temperatures (300–350 °C) markedly reduces the interfacial resistance, has been practically available.[107,108]

Recently, several approaches have been proposed to decrease the resistance for the interfacial Na^+-transfer for the electrochemical Na-plating/stripping reaction to a reasonable value by means of interfacial engineering. Zhou *et al.* ascribed the poor wetting ability of NZSP with Na metal to the high interfacial resistivity and prepared a thin interfacial interlayer by intentionally heating NZSP at 380 °C in contact with Na melt.[282] The amorphous surface film formed by the reductive reaction of NZSP was found to show good wettability against Na, allowing for efficient Na-plating/stripping with a lowered interfacial impedance. The following studies on improving the surface wettability of NZSP with Na exemplified several effective coatings, including AlF_3,[283] TiO_2,[284] and a Na–SiO_2 composite.[285] Some research groups also reported on the improvement of wettability by adding a specific additive to NZSP, such as $Na_2B_4O_7$,[197] $BaTiO_3$,[286] and CuO.[287] It should be pointed out that those coated compounds do not work as they are but are surely bound to be reduced in contact with Na metal, and hence, the detailed mechanism for each system has not been clarified yet. Lu *et al.* exploited the combinatorial strategy of the surface coating with SnO_2 and a 3D-porous NZSP scaffold.[288] The marked drop in interfacial resistance was achieved due to the drastic increase in the contact area between NZSP and Na. However, one should keep in mind that such an uneven interface may facilitate dendrite formation by the concentrated electric field at the projecting tips.[289,290]

More simply, the high-pressure compression of Na metal onto NZSP is also effective to reduce the interfacial resistance; Pervez *et al.* investigated the effects of external pressure during the electrochemical tests on the impedance of the Na-plating/stripping reaction and realized that the higher pressure applied to the Na|NZSP|Na sandwich led to a lower impedance.[291] What is more, it was revealed that the continuous high-pressure loading is not necessary and that a moderate compression (~0.25 MPa) is enough to maintain the low interfacial impedance during cell operation once a thorough contact between NZSP and Na metal is established by an initial high-pressure compression in assembling the cell, as shown in Figs. 9(a) and 9(b).[292] The resultant specific areal resistivity for the interfacial charge transfer was estimated at 14 Ω cm^2 at 25 °C by pressing at 30 MPa, compared to 660 Ω cm^2 without compression. Note that the NZSP SE for this investigation was performed on the 1 mm-thick NZSP pellet prepared via the CS process at 1270 °C for 12 h. The surfaces were mirror-polished, followed by annealing at 1100 °C to recover the surface damaged by the polishing step; otherwise, the cell is plagued by a significantly large interfacial resistivity. It was also confirmed that the NZSP sample prepared via SPS (1210 °C) followed by annealing at 1000 °C exhibited a similar interfacial resistivity of 7–10 Ω cm^2 at 25 °C by pressing the Na|NZSP|Na cell at 30 MPa. Unfortunately, our attempt to apply a high-pressure loading of Na foils onto the above-mentioned NZSP film prepared via tape casting failed because of the fragility of 20–30 μm-thick films.

The remarkable improvement of the interfacial Na^+-transfer resistivity by uniaxial compression is attributable to (i) the increase of Na/NZSP contact area due to the ductile characteristics of Na [Fig. 9(c)] and (ii) the formation of an interphase that allows efficient Na-plating/stripping.[292] The nature of interphase still remains elusive, yet the X-ray photoelectron spectroscopy (XPS) profiles [Fig. 9(d)] indicate the presence of reduced species on the NZSP surface, as with the reaction between NZSP and molten Na at 380 °C mentioned earlier.[282] Since the impedance spectrum for the Na|NZSP|Na cells pressed at 30 MPa was found to rarely change for up to two weeks, the formed interphase is stable for a long period of time.[292]

The viability of NZSP SEs sintered with an NNP glass additive in combination with a Na metal anode was examined in a similar fashion. The electrochemical tests were representatively carried out on the 10 wt. % NNP-containing NZSP pellet sintered at 990 °C by SPS. This type of NZSP exhibited a pronounced impact of the annealing temperature after surface polishing on the interfacial resistance at Na/NZSP, as displayed in Figs. 9(e) and 9(f).[293] Without annealing, the interfacial resistance was assessed to be >15 kΩ cm^2 at 25 °C even with high-pressure pressing at 30 MPa, while it diminished dramatically by the post-annealing, resulting in 19 Ω cm^2 at annealing temperature of 1000 °C. It is deduced that the mirror-polishing process with abrasive powders (typically, α-Al_2O_3 or SiC) in a coolant oil inflicts serious damage on the outermost surface of NZSP sinters upsetting the grain packing and compromising the crystallinity, and hence, the thermal treatment at a relatively high temperature is necessary to retrieve a good NZSP surface [Fig. 9(g)].

Figure 10 and Table II compare the interfacial resistances and activation energy values for the charge transfer upon Na-plating/stripping at the interfaces between the Na anode and various electrolytes. As the pressure in assembling a symmetric Na|NZSP|Na cell should have a non-negligible effect even when the NZSP is subjected to surface modification to improve the wettability against Na, a fair comparison can be permitted within the data obtained in our group. It might be remarked that the additive-free NZSP offers lower interfacial resistance than the NZSP containing impurities. Meanwhile, except for the NZSP sintered with the aid of NNP glass, the activation energy values for Na/NZSP fall within 0.4–0.6 eV, which is higher than that for Na/Na-β''-alumina (0.28–0.40 eV).[292,294]

In the case of organic liquid electrolytes, the interfacial resistance for Na-plating/stripping is composed of the charge transfer resistance as well as the resistance of a solid electrolyte interphase (SEI) layer, resulting in 175 Ω cm^2 at 25 °C in 1M $NaPF_6$ in ethylene carbonate/dimethyl carbonate (EC/DMC).[295] Besides, the resistance gradually increases to 300 Ω cm^2 after 96 h due to the growing SEI film caused by the successive decomposition of EC/DMC on the Na metal surface. According to the experimental results in our group, the interfacial resistance and activation energy have values of 200–300 Ω cm^2 and 0.6–0.8 eV, respectively, which are much higher than those estimated for the Na/NZSP and Na/Na-β''-alumina interfaces (Fig. 10).

Despite the acceptable interfacial chemistry at Na/NZSP, the use of Na metal anodes currently faces the intractable obstacle of

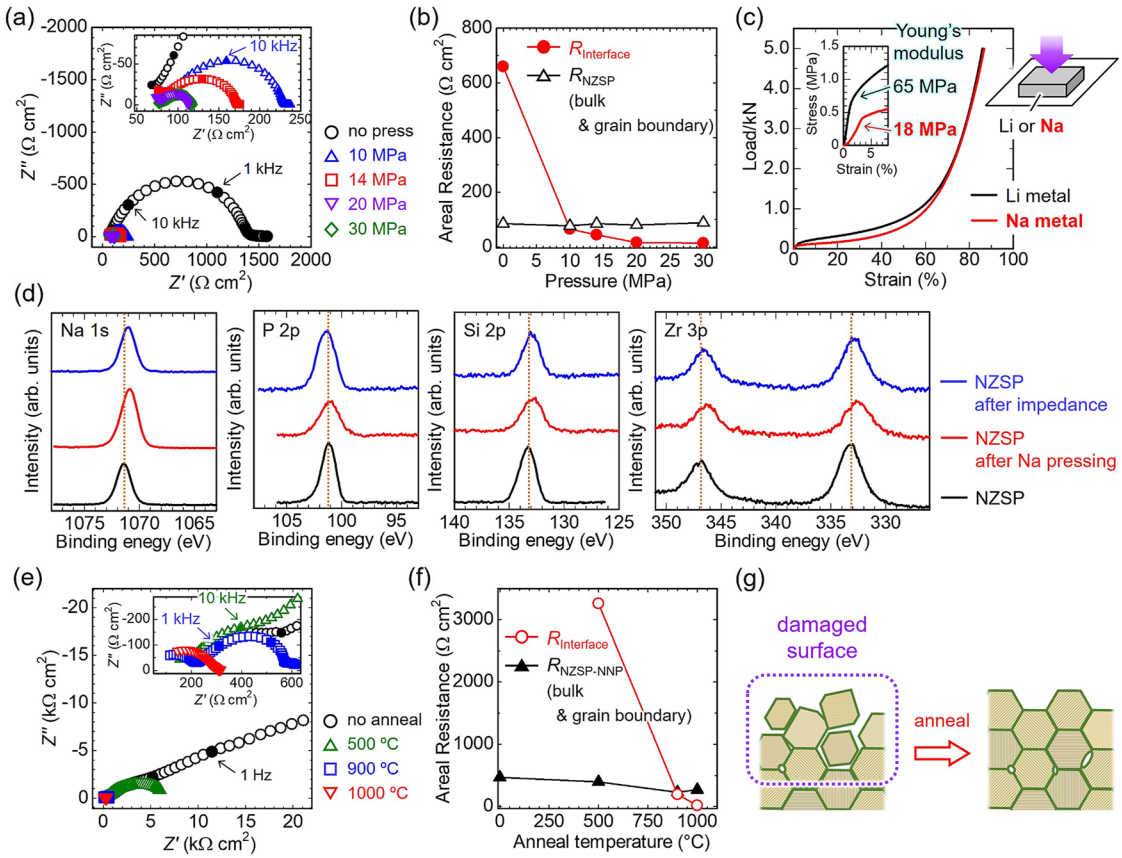

FIG. 9. Feasibility of Na metal anode with NZSP: (a) impedance spectra (25 °C; ~0.25 MPa) of the Na|NZSP|Na symmetric cells prepared by pressing at varied pressures; (b) variation of the areal resistances for the NZSP SE (R_{NZSP}) and the Na/NZSP interfacial reaction ($R_{interface}$) as a function of pre-pressing pressure; (c) mechanical behaviors of Li and Na metal blocks upon uniaxial compression (the inset shows the stress–strain curve in the small strain region based on the original dimension of each block); (d) XPS profiles of the NZSP surface before and after Na-pressing as well as impedance test; (e) impedance spectra (25 °C; ~0.25 MPa) of the Na|NZSP-NNP|Na symmetric cells with varied annealing temperature for the NZSP SE containing the NNP glass (10 wt. % NNP; SPS; 990 °C); (f) variation of the areal resistances for the NNP-containing NZSP SE ($R_{NZSP-NNP}$) and the Na/NZSP-NNP interfacial reaction ($R_{interface}$) as a function of annealing temperature; (g) schematic illustration expressing the recovery of damaged NZSP surface by annealing. Reprinted with permission from Uchida *et al.*, ACS Appl. Energy Mater. **2**, 2913 (2019). Copyright 2019 American Chemical Society.

Na dendrite growth.[281] Upon the electrochemical plating of Na corresponding to the charge step in Na-ASSBs, filament propagation across an SE layer frequently takes place, leading to a short circuit. Although the non-flammable feature of an all-oxide-based cell configuration obviates the risk of thermal runaway, fire, and explosion,[88] it causes an extremely short battery life and mortally constrains the power density and charging rate because dendrite growth is stimulated to a great extent by increasing the current density.

In the early days of ASSB research, there was an optimistic expectation that a hard and tough ceramic SE with minimized porosity could perfectly serve as a reliable protective barrier against the growth of dendrites owing to the soft and compliant mechanical properties of Na metal.[27,296,297] However, it is now commonly accepted that an SE layer with high mechanical strength and a relative density approaching 100%, even a glassy SE with a single crystal, cannot prevent the propagation of metal filaments.[270,281,289,290,298–303] This is because a great deal of volume change of a Na metal layer upon Na-plating/stripping spoils the homogeneity and flatness of the Na/NZSP interface, particularly at a high rate, and the filament propagation proceeds at parts where enhanced electric fields are applied; the intrinsic stress arising from the tip of filaments causes the spallation and transverse cracks of a rigid ceramic SE layer.[290] A recent study based on the real-time visualization of Li dendrite propagation in SEs proposed that the direct deposition of dendrites may take place, which might trigger a short circuit in another scenario.[304] Hence, research efforts have been dedicated to preventing dendrite growth and the resultant short circuit.

One benchmark to evaluate the durability of an SE against dendrite growth is the highest current density at which the Na-plating/stripping is stably repeated, termed "critical current density (CCD)."[305,306] Here, it must be emphasized that the determination of CCD for each system is highly associated with the experimental conditions, such as the quantity of electricity for a single step

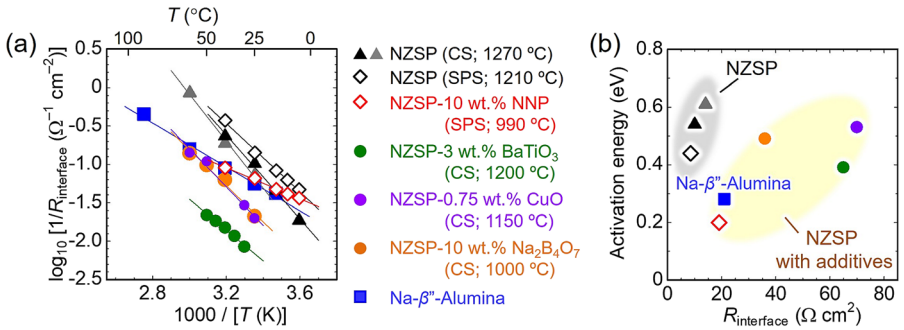

FIG. 10. Comparison of interfacial Na^+-transfer capabilities upon Na-plating/stripping at interfaces between Na and different SEs: (a) Arrhenius plots of the reciprocal interfacial resistivities at different Na/SE interfaces (see also Table II); (b) relationship between the interfacial resistivity and activation energy for different SEs.

TABLE II. Interfacial Na^+-transfer resistivities between various electrolytes and Na metal at room temperature and the corresponding activation energy values.

Electrolyte	Sintering agent	Sintering method	Other conditions	Interfacial resistivity (Ω cm^2)	Activation energy (eV)	Reference
NZSP	···	CS	···	10–14	0.54–0.61	292
NZSP	···	SPS	···	7.1	0.44	293
NZSP	NNP glass	SPS	···	19	0.20	293
NZSP	$Na_2B_4O_7$	CS	···	36	0.49	196
NZSP	CuO	CS	···	70	0.53	287
NZSP	$BaTiO_3$	CS	···	65	0.39	286
NZSP	···	CS	TiO_2-coating[a]	101[b]	···	284
NZSP	···	CS	Na–SiO_2 electrode[c]	101	···	285
Ca-NZSP	···	CS	Porous SE[d]/SnO_2 coating[e]	275	···	288
Na-β''-alumina	···	CS	···	21	0.28	292
1M $NaPF_6$ in EC/DMC	···	···	···	175 (1 h)[f] 300 (96 h)[g]	···	295

[a]The SE surface was coated with TiO_2 by atomic layer deposition (ALD).
[b]Measured at 23 °C.
[c]Na–SiO_2 composite anode was employed.
[d]Na anode was impregnated into the 3D porous SE layer.
[e]The porous SE surface was coated with SnO_2 by the solution process.
[f]Measured 1 h after the cell preparation.
[g]Measured 96 h after the cell preparation.

of electrodeposition and the thickness of an SE layer. Concerning the former, it is natural that dendrite growth is slower when the quantity of electroplated metal is small. It is of great importance to signify the quantity of electricity as a unit of "mAh cm^{-2}" or "C cm^{-2}" (1 mAh cm^{-2} equals 3.6 C cm^{-2}) for each step. The latter factor is rather complicated; the thicker SE layer prevents the short circuit more effectively while at the same time increasing the resistivity of the SE layer, resulting in faster dendrite growth at a more enhanced electric field applied at the tips of dendrites.[289,290] In addition, it has been disclosed that the pressure applied to a monolithic cell during charge/discharge is a critical factor in dominating CCD as well because the void formation upon Na-stripping causes an inhomogeneous electric field on the Na surface, which can be expelled by the continual compression.[307,308] Accordingly, it is not reasonable to compare the CCD values of different SEs unless all the conditions are identical including, the specific areal cell resistance.[309]

Figure 11 summarizes the CCD test results regarding a series of NZSP SEs with a thickness of ~1 mm prepared in our group.[292,293] The NZSP pellet prepared by the CS process without any additives was assembled into a symmetric Na|NZSP|Na cell in the manner described earlier, which showed a total cell resistivity of 72 and 32 Ω cm^2 at 25 and 90 °C, respectively. The CCD test results with a fixed duration for each Na-plating or stripping step of 30 min are shown in Figs. 11(a) and 11(b). Under this condition, the CCD was assessed as 0.8 and 2–3 mA cm^{-2} at 25 and 90 °C, respectively. In the meantime, the CCD at 90 °C for the identical NZSP was measured to be as high as 5 mA cm^{-2} when the quantity of electricity per step was restricted to 0.5 mAh cm^{-2}, as indicated in Fig. 11(c). These results clearly enlighten us about the ambiguous definition of CCD unless

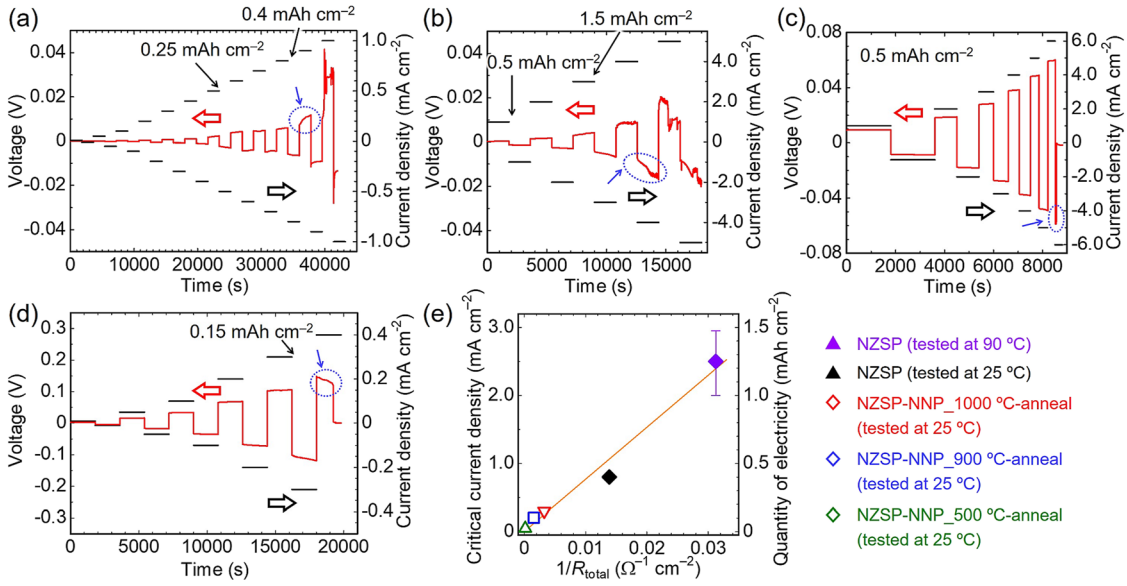

FIG. 11. Short-circuit stabilities of the NZSP (CS; 1270 °C; 1 mm thick) and NZSP-NNP (10 wt. % NNP; SPS; 990 °C; 1 mm thick) SEs as a function of current density for Na-plating/stripping: (a)–(c) galvanostatic cycling results of the Na|NZSP|Na cell prepared by pressing at 30 MPa measured at (a) 25 °C and (b) and (c) 90 °C with [(a) and (b)] the constant duration time of 1800 s and (c) the constant electric charge of 0.5 mAh cm^{-2} (1.8 C cm^{-2}) for each step; (d) voltage profile of the Na|NZSP-NNP|Na cell prepared by pressing at 30 MPa measured at 25 °C with increasing current density (duration time per step: 1800 s); (e) relationship between the reciprocal total resistivity and critical current density for different Na|SE|Na symmetric cells. Reprinted with permission from Uchida *et al.*, ACS Appl. Energy Mater. **2**, 2913 (2019). Copyright 2019 American Chemical Society.

all the test conditions are unified because it is quite obvious that the CCD value increases by decreasing the amount of electroplated Na per step and vice versa. From the standpoint of an equivalent quantity of Na electrodeposition, the specific areal capacity of 0.5 mAh cm^{-2} corresponds to the mass loading of ~5 mg cm^{-2} for a cathode active material with ~100 mAh g^{-1} (e.g., NVP), which is far lower as compared with the capacities of the present commercial LIBs as well as the launching Li-ASSBs.[44,310–312]

The capability of Na-plating/stripping as a function of current density for the NZSP sintered with NNP glass additive (SPS at 990 °C followed by annealing at 1000 °C) is also given in Fig. 11(d).[293] Despite the Nb-based impurity,[189] the feasibility of the NNP-added NZSP SE for Na metal anode is demonstrated, while the larger total cell resistivity resulted in a larger polarization and, thereby, a lower CCD of 0.4 mA cm^{-2} than the aforementioned additive-free NZSP.

In Fig. 11(e), the CCD values obtained for the symmetric cells assembled with different NZSP SEs (1 mm-thick) fixing the duration time per step are plotted as a function of the reciprocal total cell resistance.[292] Although some deviations are observed, it is plausible that there is a linear relationship between the two factors. In other words, the larger polarization for the electrodeposition of Na arising from the higher cell resistance causes faster filament propagation across the SE layer, leading to a lower CCD. Once infant metal filaments form in an SE, each filament grows up at an accelerated rate simultaneously with the spallation of the SE, and there are no ways to recover the damaged SE layer. Consequently, the increase in SE thickness might retard the deterioration of ASSBs but cannot be a perfect solution to the short circuit issue. On the contrary, the decrease in cell resistance caused by replacing the thick NZSP SE with a thinner NZSP film prepared via tape-casting might be able to prohibit the initiation of nascent filaments. At least, the cell configuration based on the thin layers of electrodes and SE that resemble MLCCs (Fig. 1) requires a relatively small capacity of each Na electrode, which limits the quantity of electricity for the single charging step, possibly pushing up the CCD.

However, the implementation of Na metal anodes also confronts many difficulties from the viewpoint of manufacturing in practice. Most significantly, NZSP films prepared via tape casting are too brittle to press a Na foil at high pressure, where an NZSP film is exposed to not only an axial pressure but also a friction-induced shear stress due to the ductile behavior of Na metal [see Fig. 9(c)].[292] In addition, the extension of a Na foil by pressing causes a short circuit by enveloping an SE layer during the production process, and the sticky nature of Na also makes the lamination process difficult. Some existing ideas concerning Na metal anodes have the potential to address these issues: *in situ* Na plating,[312] moldable composite-type Na,[313] and infiltration of liquefied Na into a 3D-porous SE layer.[288] These strategies might be beneficial for ensuring good cycleability by loading excess Na relative to the cathode capacity and mitigating the volume change during charge/discharge. Contrarily, there are drawbacks traced to the chemical nature of Na: the whole manufacturing process of Na-ASSBs is obliged to be performed in a carefully controlled atmosphere because of the considerably high reactivity of Na metal, which inflates the production cost. The low melting point

of Na (~97 °C) imposes a stringent limitation on the operating temperature as well.

Given the above-mentioned constraints of the Na anode, the substitution of another anode candidate for Na at the expense of capacity is a feasible way in the case of ASSBs based on tape-casting technology. The preceding studies on SIBs with an organic liquid electrolyte have developed a variety of anode materials ranging from insertion-type to alloying- and conversion-type electrodes.[314–316] According to the criteria for choosing electrode candidates for ASSBs described previously, alloying- and conversion-type anode materials should be excluded. Hard carbon is the first in line for an anode of SIBs with a liquid electrolyte owing to its high electronic conductivity, high capacity reaching beyond 400 mAh g^{-1},[317] low operational potential close to Na^+/Na redox,[318,319] excellent initial Coulombic efficiency over 90%,[320,321] and good cycleability.[322] The extremely low volume change during sodiation/desodiation thanks to copious pores and voids is also eligible for ASSBs. Unfortunately, no publication can be found at this moment regarding the hard carbon anode implemented in an oxide-based Na-ASSB, let alone a NASICON-based one. This is probably because the reductive nature of carbon is liable to deteriorate the surfaces of oxide-based SEs during the sintering process, establishing intimate contacts between carbon and SE. Very recently, the group at Toyota Motor Corp. reported on the superb electrode performance of hard carbon in tandem with the specific carborane-based SE bearing the high Na–ion conductivity (2×10^{-2} S cm^{-1} at 25 °C) as well as salient plasticity, $Na(CB_9H_{10})_{0.7}(CB_{11}H_{12})_{0.3}$.[323] They verified that the Na-ASSB assembled with a $Na_{0.7}Mn_{0.5}Ni_{0.2}Co_{0.3}O_2$ cathode was capable of delivering an areal capacity higher than 1 mAh cm^{-2} at 10 mA cm^{-2}, which is unachievable with a Na metal anode as discussed earlier (see also Fig. 11). This result attests to the brilliant prospect of hard carbon anodes for Na-ASSBs, and technological advancement in interfacial engineering of hard carbons and NZSP is highly desired.

More feasible anode alternatives are the NASICON-type compounds, such as $NaTi_2(PO_4)_3$[256,257] and $NaZr_2(PO_4)_3$.[324] Among them, the use of the V^{3+}/V^{2+} redox couple of NVP,[261] which is introduced as a cathode candidate previously, has been explored for Na-ASSBs in association with a NZSP SE.[265,266] NVP can additionally accommodate one Na^+ ion per formula unit to be $Na_4V_2(PO_4)_3$ at 1.6 V (vs Na^+/Na), corresponding to the theoretical capacity of 58.8 mAh g^{-1}. Accordingly, the all-NASICON-based NVP|NZSP|NVP symmetric cell can be fabricated, which has the potential to be operated at ~1.8 V.[261] Aside from the NASICON-type materials, the zero-strain anode of P2-type layered $Na_{0.66}[Li_{0.22}Ti_{0.78}]O_2$ and its analog is deemed as a highly promising candidate,[211–213] since it can be prepared by heating in air by contrast to NVP, which requires a reductive condition for synthesis.

VI. FABRICATION OF NASICON-BASED Na-ASSBs VIA TAPE CASTING

The technological evolution of Li-ASSBs has stayed ahead of their Na–ion counterparts. The first Li-ASSB was traced to the halide-based Li|LiI|AgI cells in 1969.[325–327] In 1983, the trailblazing Li-ASSB, founded on an oxide-based SE, amorphous $Li_{3.6}Si_{0.6}P_{0.4}O_4$, was engendered by the researchers at Hitachi, Ltd.[328] The $Li|Li_{3.6}Si_{0.6}P_{0.4}O_4|TiS_2$ ASSB offered an operational voltage of ~2.5 V with a cycleability of ~2000 times. However, interfacial engineering of those incipient Li-ASSBs was thoroughly based on gas-phase methodologies, viz., vacuum deposition (VD), radio frequency (RF) sputtering, and chemical vapor deposition (CVD), to make intimate contacts between electrodes and SE.[325–328] After a while, in 1999, Birke *et al.* developed the whole oxide-based Li–ion ASSB with the cell configuration of $Li_4Ti_5O_{12}|Li_{1.3}Al_{0.3}Ti_{1.7}(PO_4)_3|LiMn_2O_4$ by means of a ceramic processing technique with large-scale producibility: cold-pressing of three independent ceramic films followed by a single co-firing step with the sintering aids of $LiBO_2$ and LiF.[329] This seminal work paved the way for the ensuing innovative research on oxide-based Li- and Na-ASSBs.

As already mentioned, the most significant but arduous process for manufacturing ASSBs is to establish intimate contacts between electrode and SE components both at the electrode/electrolyte interlayer and at interparticles inside the electrode layers because SE is regularly added to enhance the ionic transportation within the electrode layer. In addition, conductive agents, most likely carbonaceous species, must be added as well to endow the electrode layer with electronic conductivity. As such, one ion-conducting layer of SE is sandwiched with a pair of redox-active layers imbued with both ion- and electron-conductivity to obtain an ASSB cell. Moreover, the cell formulation should be arranged so that the volume change during charge/discharge cycles does not exacerbate the interfacial contact to afford the battery longevity,[43–45,75–78] for example, by optimizing the thickness of each layer, introducing an exquisite microstructure, and adding a specific compound that can offset the intrinsic stress while maintaining structural integrity as a whole.

It is important to take additional care of the SE component involved in electrode layers in terms of not only the content[330–334] but also the particle size (and shape).[335–337] The ionic conductivity of an electrode layer is enhanced by increasing the volumetric ratio of SE, which in turn decreases the specific capacity due to the lowered loading mass of active materials. It was reported that the smaller particle size empowers SE to impart higher ionic conductivity to an electrode layer with a lower volumetric fraction of SE.[335–337] Depending on the kinds of electrode active materials and SEs, as well as their particle sizes, the increment in ionic conductivity of an electrode layer is to be saturated at a certain volume ratio of added SEs, which should be determined experimentally for each system. As the optimization must be performed in association with the aspect of electronic conductivity assisted by electro-conductive aids, the previous studies on Li-ASSBs suggested that the optimal volume fraction of SE normally lies in the range of 40%–50% on the premise of a random mixture.[330–334]

On top of those constructional aspects, special attention should be paid to the chemical compatibility of an electroactive material and SE pairing. On the one hand, the pair of two materials must remain unreactive with each other at the interface throughout the manufacturing process involving thermal treatment, while on the other hand, the interfacial charge transfer reaction is required to be fast enough, together with low areal interfacial resistivity, to ensure the good rate capability of an ASSB at a practical level. The former point is closely correlated with the manufacturing strategy for ASSBs because thermal treatment at a higher

temperature leads to a greater risk that mutual diffusion of constituting elements takes place,[338,339] which may become an ion blocking layer[340,341] and in turn associate with the latter point. In addition, unfavorable electrochemical reactions at interfaces may occur upon charging and discharging, resulting in a passivation interphase and/or physical isolation of electrode/SE interfaces.[342–345] For instance, Delluva *et al.* manifested that trace quantities of Li_2CO_3 on the surface of garnet-type $Li_7La_3Zr_2O_{12}$ SE crystallites, which are formed immediately upon being exposed to air, were electrochemically decomposed in the cathode layer concomitantly with the evolution of O_2 and CO_2 gases, causing interfacial delamination.[342] Hence, the manufacturing strategy available and suitable for an intended ASSB hinges on a combination of electroactive materials and SE. It should be noted that an incompatible electrode/SE pair is not necessarily non-useable for ASSBs; there are some tactics to circumvent it, like the surface coating of electroactive materials with a protective layer.[202–204,344–355]

The general procedure to prepare a composite electrode for conventional LIBs with a liquid electrolyte, where a slurry mixture of electroactive materials, conductive agents, and binders is cast on a conductive substrate such as Al and Cu foils, is applicable to form an electrode layer on SE in the case of ASSBs. Several techniques, such as screen printing, doctor blading, and spin coating, have been employed for depositing the slurry mixture of electroactive materials, electrolytes, conductive agents, and binders dispersed in a solution onto SE surfaces.[333,334,356–358] Differently from conventional LIB electrodes, the deposited electrode layer needs to be subjected to not only drying but also thermal treatment at high temperatures for sintering to ameliorate interparticle contacts.

With respect to the manufacturing strategy based on tape casting, there are three approaches to stacking the electrode and SE layers, as illustrated in Fig. 12(a). Here, only one interlayer stacking (cathode/SE or anode/SE) is taken into account for simplicity. In the first strategy (Strategy I), the two ceramic films are independently sintered, followed by unifying them using a reactive adhesive that promotes the coalescence of two sheets as a "glue."[359–363] The coalescence capability of the two films at low temperatures and the interface (or interphase) properties in terms of ion transfer are crucial in this case. The advantage lies in the flexible sintering conditions for the individual films and the lower risk of mutual diffusion if coalescence is possible at a low temperature. In the second (Strategy II), either the electrode or SE layer that needs the higher sintering temperature is processed in advance, on which a composite slurry containing the other component is deposited, followed by the second sintering step. Compared to the first strategy, there are higher risks of degradation of an initially sintered layer and mutual diffusion at the interface.[338,339] Another drawback is the possibility of fracturing and exfoliation of a second layer due to the mismatch of shrinkage during the second sintering step.[364–366] The third one (Strategy III) is the simplest, in which a pair of electrodes and

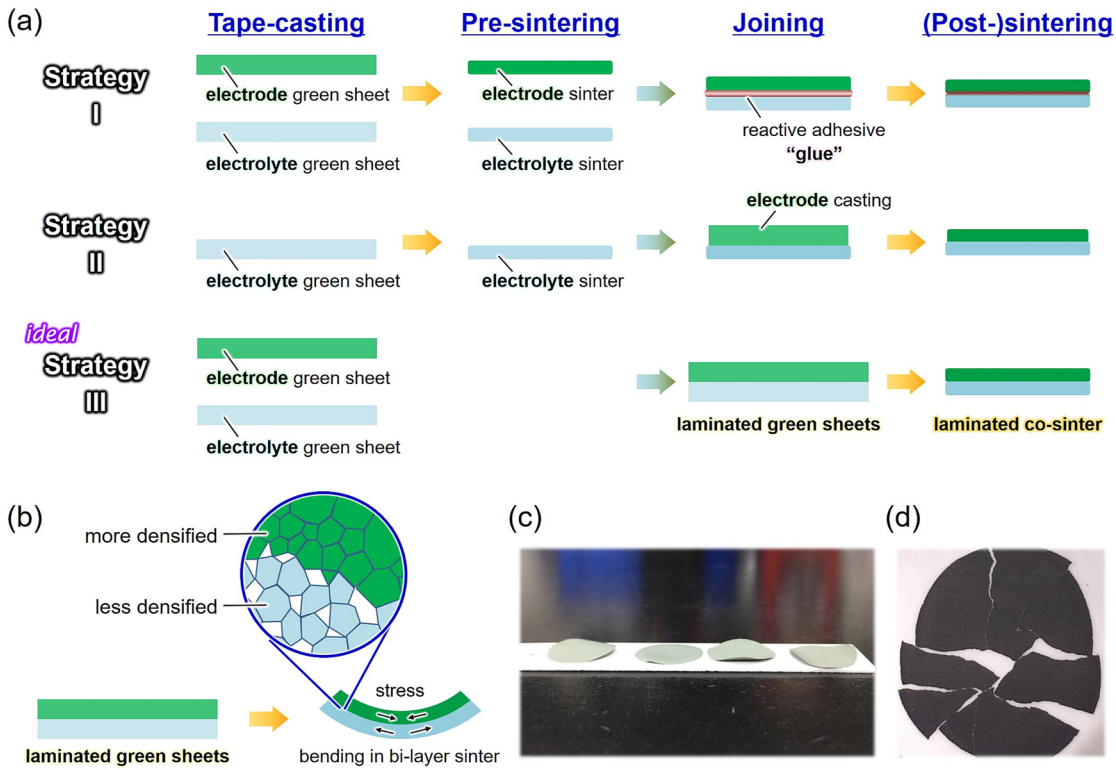

FIG. 12. Processing of bi-layer ceramic sheets via tape casting: (a) three manufacturing strategies for bi-layer stacking; (b) schematic illustration showing the issue of preparing bi-layer films due to horizontal shear force during thermal treatments; (c) and (d) photographs of examples of failures to produce bi-layer films.

SE green sheets are laminated, followed by a single sintering process favorably in the air or under a N_2 atmosphere with moderate purity. This is an ideal procedure in terms of its applicability to a multi-layer cell configuration and its large-scale producibility at a low cost, which is, however, fairly difficult in most cases. One reason is that the modest difference in in-plane shrinking degree in drying and debinding processes between the two sheets readily makes a bi-layer sheet curl and warp due to its flexible nature [Figs. 12(b) and 12(c)].[364–366] Even when a bi-layer sheet is forced to be flat during these treatments, the following sintering process makes it fracture due to the horizontal shear force arising from the different shrinking behaviors and thermal expansion coefficiencies between the two components, as exemplified in Fig. 12(d). In addition, as the sintering temperature should be on the higher side, the reactivity and interlayer diffusion should be more pronounced. Therefore, it is indispensable for the co-sintering process to carefully identify the optimal conditions in each step in addition to choosing a rational combination of electrode material and an SE. As already pointed out, the adjustment of preparation condition parameters and the identification of feasible combinations are literally matters of trial and error.

Although MLCCs are widely produced via tape casting accompanied by co-sintering,[93–99] very few reports can be found concerning a multi-layer ASSB, despite a few reports on a tri-layer cell.[367–379] Our attempt to fabricate all-oxide-based Na-ASSBs by the co-sintering strategy is displayed in Fig. 13. According to the discrete NZSP and NVP films prepared with NNP glass additive via tape casting described earlier, the optimal condition to minimize the mismatch of in-plane shrinkage during sintering was found. Sintering of 10 wt. % NNP-containing NZSP and 5 wt. % NNP-containing NVP at 900–1000 °C yielded well-sintered films with similar degrees of shrinkage, as shown in Fig. 13(a). In light of this prospect, the tri-layer NVP|NZSP|NVP cells were prepared by sandwiching NZSP green tape with a pair of NVP green sheets (both containing 10 wt. % NNP glass) by hot pressing at 6 MPa at 50 °C, which was submitted to debinding at 400 °C and sintering at 920–1000 °C for 30 min in a 5% H_2-containing Ar atmosphere.

In contrast to the bi-layer films shown in Figs. 12(c) and 12(d), the tri-layer configuration allows an NVP|NZSP|NVP sheet to maintain the crack-free and flat morphology after debinding and sintering processes, as represented in Fig. 13(b), probably because similar shear stress was applied to both surfaces of the NZSP layer owing to the symmetric structure. In addition, the NZSP intermediate layer acted as a good supporting substrate for the NVP layers preserving their integrity during the thermal treatments, even when the single NVP layer with 10 wt. % NNP glass failed to become a crack-free sintered film [see Fig. 7(a)]. Figure 13(c) shows the microstructural morphologies and elemental mapping images of the NVP|NZSP|NVP tri-layer sheets sintered at 920–1000 °C.[380] The NZSP layer was well-densified even by sintering at as low as 920 °C, whereas the densification of NVP portions proceeded with increasing the sintering temperature. It should be pointed out that the densification degree of NZSP in the tri-layer sheet sintered at 920 °C was apparently higher than that in the mono-layer NZSP film sintered at 900–1000 °C with 10 wt. % NNP glass, as indicated in Fig. 13(d). Focusing on the elemental distribution in the tri-layer sheet [Fig. 13(c)], it is perceivable that the diffusion of V from the NVP layer to the NZSP took place, which became more distinct in the samples sintered at higher temperatures. It is, therefore, plausible that the incorporation of V into the NZSP layer accounts for the enhanced densification of NZSP. On the other hand, the diffusion of Si from the NZSP layer to NVP was found to be negligible, and hence, the sintering behavior of NVP upon heating in the tri-layer sheets was analogous to that in the mono-layer counterparts [Figs. 7(b) and 13(d)].

With regard to the interface between the NZSP and NVP layers, the two layers moderately adhered to each other to the extent that one can identify where the interface locates in the microscopic images shown in Fig. 13(c).[380] It means that further effort should be dedicated to optimizing the co-sintering conditions in this tape-casting process. The impedance spectra of the tri-layer sheets consisted of a single deviated semicircle and a slope region at low frequencies, which were incapable of isolating the respective ionic transport components of NZSP and NVP.[380] The total conductivity values of the tri-layer samples were calculated to be >10 times higher than the value assessed from the sum of resistivity for the three layers. It is, therefore, likely that the diffusion of V into the NZSP layer as well as the imperfect NVP/NZSP interfaces were responsible for the extremely high total resistivity. Meanwhile, the cyclic voltammetry measurement conducted on the tri-layer NVP|NZSP|NVP cell co-sintered at 920 °C documented its capability as a Na-ASSB based on NASICON, demonstrating a well-defined redox couple centered at 1.7 V,[380] which is consistent with the potential difference between the redox pairs of V^{4+}/V^{3+} and V^{3+}/V^{2+} of NVP.[261,265,266,277]

VII. FUTURE CHALLENGES AND PERSPECTIVES

Whatever the kind of battery, research progress in developing not only new electrode and electrolyte materials with improved functionalities but also manufacturing techniques for a practical cell is of great importance to attain a breakthrough in the next-generation energy storage device. As compared with Li-ASSBs, whose commercialization has been started by ceramic companies but is still limited to microsized cells,[100–103] the research on Na-ASSBs is still at an incipient stage, apart from considering the production cost, let alone oxide-based Na-ASSBs. However, the oxide-based Na-ion SEs represented by Na-β/β''-alumina and NASICON have the advantage over their non-oxide-based and Li–ion counterparts owing to deep understandings of their physicochemical properties and mature ceramic processing technologies. The producibility of NASICON-based ceramic films via the tape-casting process with the aid of NNP glass sheds light on the future deployment of oxide-based Na-ASSBs manufactured at a reasonably low cost, yet at the same time, it also illuminates a lot of remaining issues to be addressed. Here, we set out the future challenges and research directions of oxide-based Na-ASSBs with an eye on tape-casting technology. The other critical issues, predominantly pertaining to electrode/SE interfacial matters, have been pointed out elsewhere in previous literature.[29,33,35,43–45]

Postulating the laminated multi-layer formulation for oxide-based Na-ASSBs in a manner reminiscent of MLCCs, each electrode layer should not necessarily be thick to enhance energy density. Since the ceramic films (NZSP and NVP) described earlier started with the green tapes with 40–50 μm in thickness, each tape was able to be handled individually. However, a thinner green tape

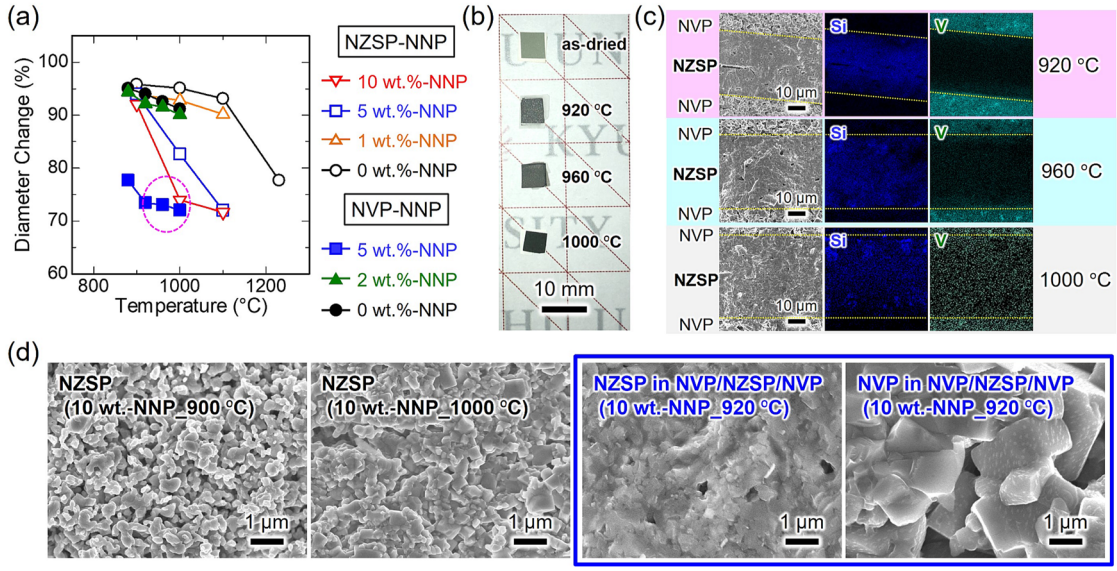

FIG. 13. Synthesis of NVP/NZSP/NVP tri-layer sheets via tape casting with the NNP glass additive: (a) shrinking behaviors of the NZSP and NVP disks with varied amounts of the NNP glass as a function of sintering temperature [see also Figs. 4(a) and 7(a)]; (b) appearances of the NVP/NZSP/NVP tri-layer sheets before and after sintering; (c) cross-sectional microstructures and elemental mapping images of the NVP/NZSP/NVP tri-layer sheets sintered at different temperatures; (d) comparison of the cross-sectional morphologies in the NZSP single layers (10 wt. % NNP; 900 °C and 1000 °C) and those in the NZSP and NVP portions of the NVP/NZSP/NVP tri-layer (10 wt. % NNP; 920 °C).

with the intent to decrease the thickness of a sintered film cannot be processed likewise. To this end, one should pursue another approach to repeatedly cast each green tape and current collector onto a stacked green laminate, followed by co-sintering, which is definitely more challenging. It is necessary to find a more effective sintering aid that drastically decreases the onset temperature of sintering while simultaneously affording a similar shrinkage behavior upon heating for the pair of an intended electrode material and NZSP.

In an alternative way, a relatively thick electrode layer (~100 μm) with high areal mass loading of electroactive materials and, thereby, high energy density is rationally designed to enable an operation at a reasonable current density. In general, the increase of an electrode layer results in a decrease in rate capability; in other words, the energy density and power density are in a trade-off relationship. An attempt to overcome this dilemma is associated with the elaboration of 3D pathways that allow for efficient charge transportation in an electrode layer.[126–130,288] However, the tape-casting process to form the MLCC-type cell formulation has an extremely low feasibility of arranging SE (and an electron conductive agent) to form a controlled microstructure; an additional process of percolating electroactive materials into a 3D porous layer is indispensable.[126–130,288]

One possible approach is to incorporate a compositional gradient into an electrode layer to maximize the transport efficiency across the layer. Sun *et al.* demonstrated the improved electrode performance of the layered lithium nickel-rich oxide cathode with a rationally-arranged compositional gradient in each particle,[381] and this approach is applicable to the electrode layer of ASSBs. Recently, Kim *et al.* fabricated a concentration-gradient composite electrode consisting of graphite and Li_2S–P_2S_5 glass ceramic electrolyte by repeatedly pelletizing three composite electrode layers with varied compositions to unify them into a single electrode for Li-ASSBs.[382,383] The gradient graphite anode, in which the higher concentration of SE is located near the SE layer, delivered superior electrode performance to the correspondent electrode without a compositional gradient. It is noteworthy that such an electrode layer with a compositional gradient is readily fabricated by tape casting: stacking a series of green tapes with varied compositions, followed by co-sintering [Fig. 14(a)].[384,385] Fine control of the compositional gradient is expected by leveraging the tape-casting process since the thickness of each layer can be flexibly modulated and the interlayer diffusion upon co-sintering can render the stepwise concentration change more gradual. Due to the lack of investigations on this topic both in Li- and Na-ASSBs, there must be considerable scope for improving ASSB performance with this strategy.

From the standpoint of materials science, it is of interest to develop a new class of additives for electrode layers that possess both electronic and ionic conductivity, namely, a good mixed conductor.[386] In a composite electrode containing electroactive materials, SEs, and electro-conductive additives, the constituent particles are not arranged to form efficient carrier pathways but are just bound to be randomly distributed. As a result, the migration routes for electrons and ions may intersect with each other, disturbing the transport of the other carriers, as portrayed in Fig. 14(b). By contrast, the mutual blocking of carriers can be circumvented by adding a single agent to a mixed conductor. In addition, this approach also

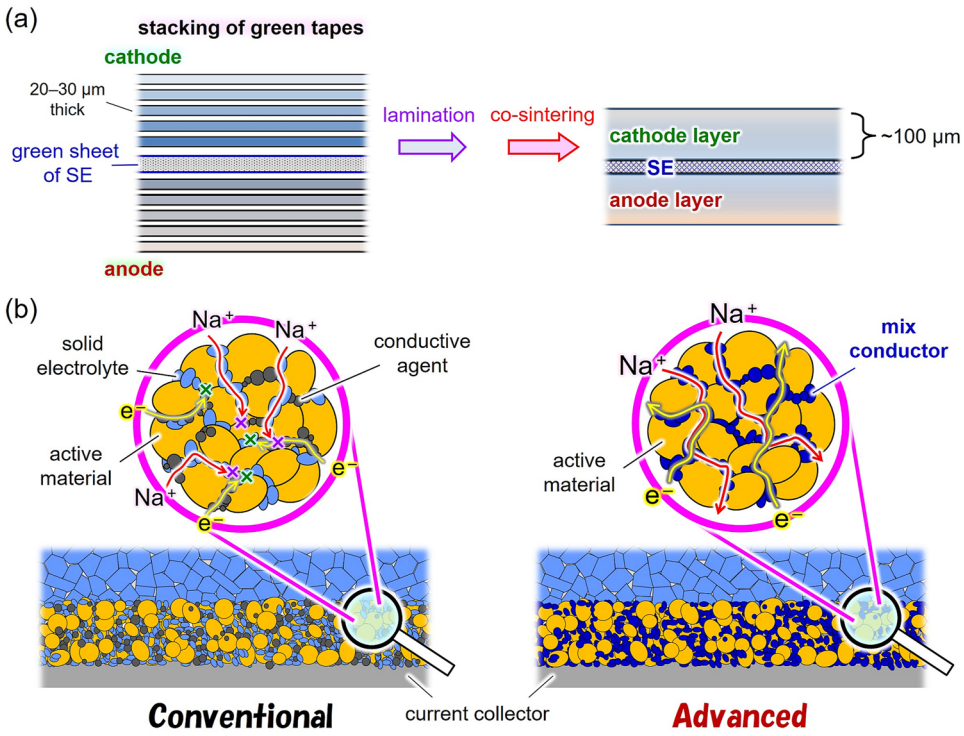

FIG. 14. Advanced technologies of manufacturing ASSBs: (a) tape-casting process to sandwich the SE with a pair of electrode layers with compositional gradient by stacking multiple green sheets with varied compositions for each electrode layer; (b) comparison between the composite electrode layer consisting of active material, conductive agent, and SE (conventional) and that consisting of active material and mixed conductor (advanced).

mitigates the concerns of unfavorable reactions between ingredients in an electrode layer and makes it easy to optimize the synthetic conditions due to the reduced parameters. For instance, thermal treatments of oxide-based constituents with reductive carbonaceous conductive agents often spoil the phase purity and decrease the sinterability, leaving too much porosity in the final product. Accordingly, the favorable mixed ion–electron conducting agents are oxide-based ceramics that can be compacted with electrode active materials by heating in air.

Some electrode active materials for LIBs and SIBs based on transition metal oxides are renowned for acquiring a pronounced mixed conducting nature by the partial insertion or extraction of alkali ions, e.g., $Li_{1-x}CoO_2$,[387] $Li_{4+x}Ti_5O_{12}$,[388] and $Na_{1-x}CoO_2$.[389] However, these compounds suffer from several constraints, such as thermal instability due to the thermodynamically unstable state and the limitation of the available potential range to hold a high mixed conductivity. Thus far, there are no potent mixed conducting agents for an electrode layer in ASSBs that we have screened for. The desirable features of mixed conducting agents involve thermal stability (favorably, processability in the air), chemical and electrochemical inertness free from redox activity, and rare-earth-free constituents. We believe that the discovery of such a new class of additives will provide a versatile platform for producing not only Li- and Na-ASSBs but also a wide variety of electrochemical devices.

To conclude this perspective, although we focus on the potential and benefits of oxide-based Na-ASSBs and the tape-casting process, it does not mean that one should exclude the possibilities for a practical application of other types of ASSBs prepared via different approaches. On the contrary, individual battery configurations and synthetic approaches have their own virtues from multifaceted viewpoints. It has commonly occurred in history that an innovation in a different field offered a game-changing technology for a system that had been deemed hopeless until then. Hence, we encourage researchers to keep devoting their efforts to a multidisciplinary view so as to push forward all the existing battery systems and manufacturing techniques.

ACKNOWLEDGMENTS

The authors acknowledge Dr. He Wang, Mr. Keisuke Okubo, Mr. Yasuhiro Uchida, and Mr. Takehiro Kashihara for their contributions to the studies described herein. Special acknowledgments go to all co-workers and collaborators as well. The authors also wish to acknowledge the financial support such as Grant-in-Aid for Scientific Research on Innovative Areas "Mixed Anion" (Grant Nos. JP16H06439, JP16H06440, and 17H05491) and Grant-in-Aid for Scientific Research (A) (Grant No. 19H00828) from the Japan Society for the Promotion of Science (JSPS) as well as the

Elements Strategy Initiative to Form Core Research Center, Ministry of Education, Culture, Sports, Science, and Technology (MEXT), Japan.

AUTHOR DECLARATIONS

Conflict of Interest

The authors have no conflicts to disclose.

Author Contributions

George Hasegawa: Writing – original draft (lead). **Katsuro Hayashi**: Writing – review & editing (equal).

DATA AVAILABILITY

The data that support the findings of this study are available within the article.

REFERENCES

[1]T. Nagaura, Prog. Batteries Battery Mater. **10**, 209 (1991).
[2]T. Nagaura, Prog. Batteries Battery Mater. **10**, 218 (1991).
[3]Y. Nishi, Chem. Rec. **1**, 406 (2001).
[4]A. Yoshino, Angew. Chem., Int. Ed. **51**, 5798 (2012).
[5]F. C. Laman and K. Brandt, J. Power Sources **24**, 195 (1988).
[6]M. Winter, B. Barnett, and K. Xu, Chem. Rev. **118**, 11433 (2018).
[7]M. Li, J. Lu, Z. Chen, and K. Amine, Adv. Mater. **30**, 1800561 (2018).
[8]P. G. Bruce, S. A. Freunberger, L. J. Hardwick, and J.-M. Tarascon, Nat. Mater. **11**, 19 (2012).
[9]J. B. Goodenough and K.-S. Park, J. Am. Chem. Soc. **135**, 1167 (2013).
[10]D. Larcher and J.-M. Tarascon, Nat. Chem. **7**, 19 (2015).
[11]C. J. Jafta, Curr. Opin. Electrochem. **36**, 101130 (2022).
[12]S. Tong, T. Fung, M. P. Klein, D. A. Weisbach, and J. W. Park, J. Energy Storage **11**, 200 (2017).
[13]G. Zubi, R. Dufo-López, M. Carvalho, and G. Pasaoglu, Renewable Sustainable Energy Rev. **89**, 292 (2018).
[14]B. Zakeri and S. Syri, Renewable Sustainable Energy Rev. **42**, 569 (2015).
[15]S. Troy, A. Schreiber, T. Reppert, H.-G. Gehrke, M. Finsterbusch, S. Uhlenbruck, and P. Stenzel, Appl. Energy **169**, 757 (2016).
[16]X. Zhang, L. Li, E. Fan, Q. Xue, Y. Bian, F. Wu, and R. Chen, Chem. Soc. Rev. **47**, 7239 (2018).
[17]G. Harper, R. Sommerville, E. Kendrick, L. Driscoll, P. Slater, R. Stolkin, A. Walton, P. Christensen, O. Heidrich, S. Lambert, A. Abbott, K. Ryder, L. Gaines, and P. Anderson, Nature **575**, 75 (2019).
[18]E. Fan, L. Li, Z. Wang, J. Lin, Y. Huang, Y. Yao, R. Chen, and F. Wu, Chem. Rev. **120**, 7020 (2020).
[19]S. P. Ong, V. L. Chevrier, G. Hautier, A. Jain, C. Moore, S. Kim, X. Ma, and G. Ceder, Energy Environ. Sci. **4**, 3680 (2011).
[20]V. Palomares, P. Serras, I. Villaluenga, K. B. Hueso, J. Carretero-González, and T. Rojo, Energy Environ. Sci. **5**, 5884 (2012).
[21]S.-W. Kim, D.-H. Seo, X. Ma, G. Ceder, and K. Kang, Adv. Energy Mater. **2**, 710 (2012).
[22]M. D. Slater, D. Kim, E. Lee, and C. S. Johnson, Adv. Funct. Mater. **23**, 947 (2013).
[23]C. Delmas, Adv. Energy Mater. **8**, 1703137 (2018).
[24]I. Hasa, S. Mariyappan, D. Saurel, P. Adelhelm, A. Y. Koposov, C. Masquelier, L. Croguennec, and M. Casas-Cabanas, J. Power Sources **482**, 228872 (2021).
[25]Y. Tian, G. Zeng, A. Rutt, T. Shi, H. Kim, J. Wang, J. Koettgen, Y. Sun, B. Ouyang, T. Chen, Z. Lun, Z. Rong, K. Persson, and G. Ceder, Chem. Rev. **121**, 1623 (2021).
[26]C. Sun, J. Liu, Y. Gong, D. P. Wilkinson, and J. Zhang, Nano Energy **33**, 363 (2017).
[27]C. Zhao, L. Liu, X. Qi, Y. Lu, F. Wu, J. Zhao, Y. Yu, Y.-S. Hu, and L. Chen, Adv. Energy Mater. **8**, 1703012 (2018).
[28]W. Hou, X. Guo, X. Shen, K. Amine, H. Yu, and J. Lu, Nano Energy **52**, 279 (2018).
[29]Y. Lu, L. Li, Q. Zhang, Z. Niu, and J. Chen, Joule **2**, 1747 (2018).
[30]T. Famprikis, P. Canepa, J. A. Dawson, M. S. Islam, and C. Masquelier, Nat. Mater. **18**, 1278 (2019).
[31]H. Shen, E. Yi, L. Cheng, M. Amores, G. Chen, S. W. Sofie, and M. M. Doeff, Sustainable Energy Fuels **3**, 1647 (2019).
[32]R. Chen, Q. Li, X. Yu, L. Chen, and H. Li, Chem. Rev. **120**, 6820 (2020).
[33]W. Zhang, C. D. Zhao, and X. L. Wu, Adv. Mater. Interfaces **7**, 2001444 (2020).
[34]X. Yang, K. R. Adair, X. Gao, and X. Sun, Energy Environ. Sci. **14**, 643 (2021).
[35]Y. Ren, T. Danner, A. Moy, M. Finsterbusch, T. Hamann, J. Dippell, T. Fuchs, M. Müller, R. Hoft, A. Weber, L. A. Curtiss, P. Zapol, M. Klenk, A. T. Ngo, P. Barai, B. C. Wood, R. Shi, L. F. Wan, T. W. Heo, M. Engels, J. Nanda, F. H. Richter, A. Latz, V. Srinivasan, J. Janek, J. Sakamoto, E. D. Wachsman, and D. Fattakhova-Rohlfing, Adv. Energy Mater. **13**, 2201939 (2023).
[36]S. Gandi, V. S. C. S. Vaddadi, S. S. S. Panda, N. K. Goona, S. R. Parne, M. Lakavat, and A. Bhaumik, J. Power Sources **521**, 230930 (2022).
[37]A. Kraytsberg and Y. Ein-Eli, Adv. Energy Mater. **2**, 922 (2012).
[38]A. Manthiram, K. Chemelewski, and E.-S. Lee, Energy Environ. Sci. **7**, 1339 (2014).
[39]W. Li, B. Song, and A. Manthiram, Chem. Soc. Rev. **46**, 3006 (2017).
[40]X. Fan, L. Chen, O. Borodin, X. Ji, J. Chen, S. Hou, T. Deng, J. Zheng, C. Yang, S.-C. Liou, K. Amine, K. Xu, and C. Wang, Nat. Nanotechnol. **13**, 715 (2018).
[41]Y. You and A. Manthiram, Adv. Energy Mater. **8**, 1701785 (2018).
[42]A. Gezović, M. J. Vujković, M. Milović, V. Grudić, R. Dominko, and S. Mentus, Energy Storage Mater. **37**, 243 (2021).
[43]X. Miao, H. Wang, R. Sun, C. Wang, Z. Zhang, Z. Li, and L. Yin, Energy Environ. Sci. **13**, 3780 (2020).
[44]M. Balaish, J. C. Gonzalez-Rosillo, K. J. Kim, Y. Zhu, Z. D. Hood, and J. L. M. Rupp, Nat. Energy **6**, 227 (2021).
[45]D. A. Edelman, T. G. Brandt, E. Temeche, and R. M. Laine, Mater. Today Commun. **32**, 104009 (2022).
[46]F. B. Dias, L. Plomp, and J. B. J. Veldhuis, J. Power Sources **88**, 169 (2000).
[47]Q. Zhao, S. Stalin, C.-Z. Zhao, and L. A. Archer, Nat. Rev. Mater. **5**, 229 (2020).
[48]F. Zheng, M. Kotobuki, S. Song, M. O. Lai, and L. Lu, J. Power Sources **389**, 198 (2018).
[49]Z. Zhang, Y. Shao, B. Lotsch, Y.-S. Hu, H. Li, J. Janek, L. F. Nazar, C.-W. Nan, J. Maier, M. Armand, and L. Chen, Energy Environ. Sci. **11**, 1945 (2018).
[50]L. Fan, S. Wei, S. Li, Q. Li, and Y. Lu, Adv. Energy Mater. **8**, 1702657 (2018).
[51]R. DeWees and H. Wang, ChemSusChem **12**, 3713 (2019).
[52]Y. Kato, S. Hori, and R. Kanno, Adv. Energy Mater. **10**, 2002153 (2020).
[53]Z. Li, P. Liu, K. Zhu, Z. Zhang, Y. Si, Y. Wang, and L. Jiao, Energy Fuels **35**, 9063 (2021).
[54]L. Duchêne, A. Remhof, H. Hagemann, and C. Battaglia, Energy Storage Mater. **25**, 782 (2020).
[55]J. Popovic, D. Brandell, S. Ohno, K. B. Hatzell, J. Zheng, and Y.-Y. Hu, J. Mater. Chem. A **9**, 6050 (2021).
[56]K. Xu, Chem. Rev. **114**, 11503 (2014).
[57]S. Lee, G. Kwon, K. Ku, K. Yoon, S.-K. Jung, H.-D. Lim, and K. Kang, Adv. Mater. **30**, 1704682 (2018).
[58]G. G. Eshetu, G. A. Elia, M. Armand, M. Forsyth, S. Komaba, T. Rojo, and S. Passerini, Adv. Energy Mater. **10**, 2000093 (2020).
[59]A. Hayashi, K. Noi, A. Sakuda, and M. Tatsumisago, Nat. Commun. **3**, 856 (2012).
[60]A. Sakuda, A. Hayashi, and M. Tatsumisago, Sci. Rep. **3**, 2261 (2013).
[61]Y. Kato, S. Hori, T. Saito, K. Suzuki, M. Hirayama, A. Mitsui, M. Yonemura, H. Iba, and R. Kanno, Nat. Energy **1**, 16030 (2016).

[62]T. J. Udovic, M. Matsuo, A. Unemoto, N. Verdal, V. Stavila, A. V. Skripov, J. J. Rush, H. Takamura, and S. Orimo, Chem. Commun. **50**, 3750 (2014).
[63]T. J. Udovic, M. Matsuo, W. S. Tang, H. Wu, V. Stavila, A. V. Soloninin, R. V. Skoryunov, O. A. Babanova, A. V. Skripov, J. J. Rush, A. Unemoto, H. Takamura, and S. Orimo, Adv. Mater. **26**, 7622 (2014).
[64]W. S. Tang, A. Unemoto, W. Zhou, V. Stavila, M. Matsuo, H. Wu, S. Orimo, and T. J. Udovic, Energy Environ. Sci. **8**, 3637 (2015).
[65]W. S. Tang, M. Matsuo, H. Wu, V. Stavila, W. Zhou, A. A. Talin, A. V. Soloninin, R. V. Skoryunov, O. A. Babanova, A. V. Skripov, A. Unemoto, S. Orimo, and T. J. Udovic, Adv. Energy Mater. **6**, 1502237 (2016).
[66]W. S. Tang, K. Yoshida, A. V. Soloninin, R. V. Skoryunov, O. A. Babanova, A. V. Skripov, M. Dimitrievska, V. Stavila, S. Orimo, and T. J. Udovic, ACS Energy Lett. **1**, 659 (2016).
[67]L. Duchêne, R.-S. Kühnel, E. Stilp, E. C. Reyes, A. Remhof, H. Hagemann, and C. Battaglia, Energy Environ. Sci. **10**, 2609 (2017).
[68]R. Asakura, L. Duchêne, R.-S. Kühnel, A. Remhof, H. Hagemann, and C. Battaglia, ACS Appl. Mater. Interfaces **2**, 6924 (2019).
[69]W. Wu, Nanoscale **9**, 7342 (2017).
[70]J. Schnell, T. Günther, T. Knoche, C. Vieider, L. Köhler, A. Just, M. Keller, S. Passerini, and G. Reinhart, J. Power Sources **382**, 160 (2018).
[71]J. Schnell, F. Tietz, C. Singer, A. Hofer, N. Billot, and G. Reinhart, Energy Environ. Sci. **12**, 1818 (2019).
[72]C. Singer, J. Schnell, and G. Reinhart, Energy Technol. **9**, 2000665 (2021).
[73]K. J. Huang, G. Ceder, and E. A. Olivetti, Joule **5**, 564 (2021).
[74]K. Min, J. Electrochem. Soc. **168**, 030541 (2021).
[75]H.-K. Tian and Y. Qi, J. Electrochem. Soc. **164**, E3512 (2017).
[76]T. Yoshinari, R. Koerver, P. Hofmann, Y. Uchimoto, W. G. Zeier, and J. Janek, ACS Appl. Mater. Interfaces **11**, 23244 (2019).
[77]Y. Huang, B. Shao, and F. Han, Curr. Opin. Electrochem. **33**, 100933 (2022).
[78]A. Y. Hou, C. Y. Huang, C. L. Tsai, C. W. Huang, R. Schierholz, H. Y. Lo, H. Tempel, H. Kungl, R. A. Eichel, J. K. Chang, and W. W. Wu, Adv. Sci. **10**, 2205012 (2023).
[79]L. Liu, X. Qi, Q. Ma, X. Rong, Y.-S. Hu, Z. Zhou, H. Li, X. Huang, and L. Chen, ACS Appl. Mater. Interfaces **8**, 32631 (2016).
[80]X. Yu, L. Xue, J. B. Goodenough, and A. Manthiram, ACS Mater. Lett. **1**, 132 (2019).
[81]Y. Wang, Z. Wang, J. Sun, F. Zheng, M. Kotobuki, T. Wu, K. Zeng, and L. Lu, J. Power Sources **454**, 227949 (2020).
[82]W. Niu, L. Chen, Y. Liu, and L.-Z. Fan, Chem. Eng. J. **384**, 123233 (2020).
[83]H. Gao, L. Xue, S. Xin, K. Park, and J. B. Goodenough, Angew. Chem., Int. Ed. **56**, 5541 (2017).
[84]X. Yu, L. Xue, J. B. Goodenough, and A. Manthiram, Adv. Funct. Mater. **31**, 2002144 (2021).
[85]A. Jena, Y. Meesala, S.-F. Hu, H. Chang, and R.-S. Liu, ACS Energy Lett. **3**, 2775 (2018).
[86]A. M. Bates, Y. Preger, L. Torres-Castro, K. L. Harrison, S. J. Harris, and J. Hewson, Joule **6**, 742 (2022).
[87]G. N. Howatt, R. G. Breckenridge, and J. M. Brownlow, J. Am. Ceram. Soc. **30**, 237 (1947).
[88]D. Hotza and P. Greil, Mater. Sci. Eng. A **202**, 206 (1995).
[89]H. M. Chan, Annu. Rev. Mater. Sci. **27**, 249 (1997).
[90]M. Jabbari, R. Bulatova, A. I. Y. Tok, C. R. H. Bahl, E. Mitsoulis, and J. H. Hattel, Mater. Sci. Eng. B **212**, 39 (2016).
[91]B. Schwartz, J. Phys. Chem. Solids **45**, 1051 (1984).
[92]C. Pithan, D. Hennings, and R. Waser, Int. J. Appl. Ceram. Technol. **2**, 1 (2005).
[93]F. D. Minatto, P. Milak, A. de Noni, Jr., D. Hotza, and O. R. K. Montedo, Adv. Appl. Ceram. **114**, 127 (2015).
[94]J. Li, F. Li, Z. Xu, and S. Zhang, Adv. Mater. **30**, 1802155 (2018).
[95]J. Riegel, H. Neumann, and H.-M. Wiedenmann, Solid State Ionics **152-153**, 783 (2002).
[96]J. Will, A. Mitterdorfer, C. Kleinlogel, D. Perednis, and L. J. Gauckler, Solid State Ionics **131**, 79 (2000).
[97]D. Stöver, H. P. Buchkremer, and S. Uhlenbruck, Ceram. Int. **30**, 1107 (2004).
[98]T. L. Cable and S. W. Sofie, J. Power Sources **174**, 221 (2007).
[99]A. Sano, U.S. patent 2015/0047767A1 (19 February 2015).
[100]TDK Electronics AG, CeraCharge™ Rechargeable Multilayer Ceramic Chip Battery, available at https://www.tdk-electronics.tdk.com/en/ceracharge.
[101]TAIYO YUDEN Co., Ltd., TAIYO YUDEN Report 2020, available at https://www.yuden.co.jp/en/ir/2020ar/download/.
[102]M. Ouchi, M. Yoshioka, and T. Hayashi, U.S. patent 9368828B2 (14 June 2016).
[103]Y.-F. Yu, Y. Yao, and J. T. Kummer, J. Inorg. Nucl. Chem. **29**, 2453 (1967).
[104]J. T. Kummer, Prog. Solid State Chem. **7**, 141 (1972).
[105]R. Stevens and J. G. P. Binner, J. Mater. Sci. **19**, 695 (1984).
[106]K. Koganei, T. Oyama, M. Inada, N. Enomoto, and K. Hayashi, Solid State Ionics **267**, 22 (2014).
[107]X. Lu, G. Xia, J. P. Lemmon, and Z. Yang, J. Power Sources **195**, 2431 (2010).
[108]K. B. Hueso, M. Armand, and T. Rojo, Energy Environ. Sci. **6**, 734 (2013).
[109]J. B. Goodenough, H. Y.-P. Hong, and J. A. Kafalas, Mater. Res. Bull. **11**, 203 (1976).
[110]H. Y.-P. Hong, Mater. Res. Bull. **11**, 173 (1976).
[111]N. Anantharamulu, K. K. Rao, G. Rambabu, B. V. Kumar, V. Radha, and M. Vithal, J. Mater. Sci. **46**, 2821 (2011).
[112]Y. B. Rao, K. K. Bharathi, and L. N. Patro, Solid State Ionics **366-367**, 115671 (2021).
[113]K. Singh, A. Chakraborty, R. Thirupathi, and S. Omar, Ionics **28**, 5289 (2022).
[114]F. d'Yvoire, M. Pintard-Scrépel, E. Bretey, and M. de la Rochère, Solid State Ionics **9-10**, 851 (1983).
[115]S. Chen, C. Wu, L. Shen, C. Zhu, Y. Huang, K. Xi, J. Maier, and Y. Yu, Adv. Mater. **29**, 1700431 (2017).
[116]Z. Jian, Y. S. Hu, X. Ji, and W. Chen, Adv. Mater. **29**, 1601925 (2017).
[117]L. N. Zhao, T. Zhang, H. L. Zhao, and Y. L. Hou, Mater. Today Nano **10**, 100072 (2020).
[118]B. Singh, Z. Wang, S. Park, G. S. Gautam, J.-N. Chotard, L. Croguennec, D. Carlier, A. K. Cheetham, C. Masquelier, and P. Canepa, J. Mater. Chem. A **9**, 281 (2021).
[119]S. W. Sofie, J. Am. Ceram. Soc. **90**, 2024 (2007).
[120]L. Ren, Y.-P. Zeng, and D. Jiang, J. Am. Ceram. Soc. **90**, 3001 (2007).
[121]Y. Chen, Y. Zhang, J. Baker, P. Majumdar, Z. Yang, M. Han, and F. Chen, ACS Appl. Mater. Interfaces **6**, 5130 (2014).
[122]Y. Chen, Y. Lin, Y. Zhang, S. Wang, D. Su, Z. Yang, M. Han, and F. Chen, Nano Energy **8**, 25 (2014).
[123]R. K. Nishihora, P. L. Rachadel, M. G. N. Quadri, and D. Hotza, J. Eur. Ceram. Soc. **38**, 988 (2018).
[124]S.-W. Song, K.-C. Lee, and H.-Y. Park, J. Power Sources **328**, 311 (2016).
[125]K. Lee, S. Kim, J. Park, S. H. Park, A. Coskun, D. S. Jung, W. Cho, and J. W. Choi, J. Electrochem. Soc. **164**, A2075 (2017).
[126]K. Fu, Y. Gong, G. T. Hitz, D. W. McOwen, Y. Li, S. Xu, Y. Wen, L. Zhang, C. Wang, G. Pastel, J. Dai, B. Liu, H. Xie, Y. Yao, E. D. Wachsman, and L. Hu, Energy Environ. Sci. **10**, 1568 (2017).
[127]D. W. McOwen, S. Xu, Y. Gong, Y. Wen, G. L. Godbey, J. E. Gritton, T. R. Hamann, J. Dai, G. T. Hitz, L. Hu, and E. D. Wachsman, Adv. Mater. **30**, 1707132 (2018).
[128]C. Yang, L. Zhang, B. Liu, S. Xu, T. Hamann, D. McOwen, J. Dai, W. Luo, Y. Gong, E. D. Wachsman, and L. Hu, Proc. Natl. Acad. Sci. U. S. A. **115**, 3770 (2018).
[129]G. T. Hitz, D. W. McOwen, L. Zhang, Z. Ma, Z. Fu, Y. Wen, Y. Gong, J. Dai, T. R. Hamann, L. Hu, and E. D. Wachsman, Mater. Today **22**, 50 (2019).
[130]E. Yi, H. Shen, S. Heywood, J. Alvarado, D. Y. Parkinson, G. Chen, S. W. Sofie, and M. M. Doeff, ACS Appl. Energy Mater. **3**, 170 (2020).
[131]T. Ates, M. Keller, J. Kulisch, T. Adermann, and S. Passerini, Energy Storage Mater. **17**, 204 (2019).
[132]K. Gao, M. He, Y. Li, Y. Zhang, J. Gao, X. Li, Z. Cui, Z. Zhan, and T. Zhang, J. Alloys Compd. **791**, 923 (2019).
[133]M. Rosen, M. Finsterbusch, O. Guillon, and D. Fattakhova-Rohlfing, J. Mater. Chem. A **10**, 2320 (2022).
[134]Y. Xia, J. Li, Z. Xiao, X. Zhou, J. Zhang, H. Huang, Y. Gan, X. He, and W. Zhang, ACS Appl. Mater. Interfaces **14**, 33361 (2022).
[135]R. Moreno, Am. Ceram. Soc. Bull. **71**, 1521 (1992).
[136]R. Moreno, Am. Ceram. Soc. Bull. **71**, 1647 (1992).

[137]B. Ferrari and R. Moreno, J. Eur. Ceram. Soc. **30**, 1069 (2010).
[138]D.-H. Yoon and B. I. Lee, J. Eur. Ceram. Soc. **24**, 739 (2004).
[139]D.-H. Yoon and B. I. Lee, J. Eur. Ceram. Soc. **24**, 753 (2004).
[140]L. Ren, X. Luo, and H. Zhou, J. Am. Ceram. Soc. **101**, 3874 (2018).
[141]R. L. Coble, J. Appl. Phys. **32**, 793 (1961).
[142]W. D. Kingery, J. Appl. Phys. **30**, 301 (1959).
[143]K. C. Radford and R. J. Bratton, J. Mater. Sci. **14**, 59 (1979).
[144]R. M. German, P. Suri, and S. J. Park, J. Mater. Sci. **44**, 1 (2009).
[145]J. S. Chappell, T. A. Ring, and J. D. Birchall, J. Appl. Phys. **60**, 383 (1986).
[146]J.-M. Ting and R. Y. Lin, J. Mater. Sci. **29**, 1867 (1994).
[147]J. Ma and L. C. Lim, J. Eur. Ceram. Soc. **22**, 2197 (2002).
[148]R. J. Pugh, Adv. Colloid Interface Sci. **64**, 67 (1996).
[149]Z. Fu, U. Eckstein, A. Dellert, and A. Roosen, J. Eur. Ceram. Soc. **35**, 2883 (2015).
[150]L. E. Khoong, Y. M. Tan, and Y. C. Lam, J. Eur. Ceram. Soc. **30**, 1973 (2010).
[151]P. M. Bhatt, A. M. Kabir, M. Peralta, H. A. Bruck, and S. K. Gupta, Addit. Manuf. **27**, 278 (2019).
[152]A. K. Dubey and V. Yadava, Int. J. Mach. Tools Manuf. **48**, 609 (2008).
[153]J. A. Lewis, Annu. Rev. Mater. Sci. **27**, 147 (1997).
[154]A. Bandyopadhyay, S. C. Danforth, and A. Safari, J. Mater. Sci. **35**, 3983 (2000).
[155]P. M. Raj, A. Odulena, and W. R. Cannon, Acta Mater. **50**, 2559 (2002).
[156]Z. Fu and A. Roosen, J. Am. Ceram. Soc. **98**, 20 (2015).
[157]P. Z. Cai, D. J. Green, and G. L. Messing, J. Am. Ceram. Soc. **80**, 1929 (1997).
[158]L. A. Salam, R. D. Matthews, and H. Robertson, J. Eur. Ceram. Soc. **20**, 1375 (2000).
[159]R. Jiménez, A. del Campo, M. L. Calzada, J. Sanz, S. D. Kobylianska, B. O. Liniova, A. G. Belous, and A. V. Ragulya, J. Eur. Ceram. Soc. **38**, 1679 (2018).
[160]Y.-S. Chou and D. J. Green, J. Am. Ceram. Soc. **75**, 3346 (1992).
[161]H. Liu and S. M. Hsu, J. Am. Ceram. Soc. **79**, 2452 (1996).
[162]H. Tomaszewski, H. Węglarz, A. Wajler, M. Boniecki, and D. Kalinski, J. Eur. Ceram. Soc. **27**, 1373 (2007).
[163]S.-H. Lee, E. R. Kupp, A. J. Stevenson, J. M. Anderson, G. L. Messing, X. Li, and E. C. Dickey, J. Am. Ceram. Soc. **92**, 1456 (2009).
[164]C. Wei, X. Zhang, P. Hu, W. Han, and G. Tian, Scr. Mater. **65**, 791 (2011).
[165]K. Ren, Y. Cao, Y. Chen, G. Shao, J. Dai, and Y. Wang, Scr. Mater. **187**, 384 (2020).
[166]X. Zhang, J. Wang, J. Wen, Y. Wang, N. Li, J. Wang, and L. Fan, Ceram. Int. **48**, 18999 (2022).
[167]J.-S. Lee, C.-M. Chang, Y. I. Lee, J.-H. Lee, and S.-H. Hong, J. Am. Ceram. Soc. **87**, 305 (2004).
[168]H. Wang, K. Okubo, M. Inada, G. Hasegawa, N. Enomoto, and K. Hayashi, Solid State Ionics **322**, 54 (2018).
[169]D. Kutsuzawa, T. Kobayashi, and S. Komiya, ACS Appl. Energy Mater. **5**, 4025 (2022).
[170]J. G. Pereira da Silva, M. Bram, A. M. Laptev, J. Gonzalez-Julian, Q. Ma, F. Tietz, and O. Guillon, J. Eur. Ceram. Soc. **39**, 2697 (2019).
[171]H. Leng, J. Huang, J. Nie, and J. Luo, J. Power Sources **391**, 170 (2018).
[172]Z. M. Grady, K. Tsuji, A. Ndayishimiye, J. Hwan-Seo, and C. A. Randall, ACS Appl. Energy Mater. **3**, 4356 (2020).
[173]S. S. Zhang, J. Power Sources **164**, 351 (2007).
[174]J. D. Katz, Annu. Rev. Mater. Sci. **22**, 153 (1992).
[175]M. Omori, Mater. Sci. Eng. A **287**, 183 (2000).
[176]H. V. Atkinson and S. Davies, Metall. Mater. Trans. A **31**, 2981 (2000).
[177]R. Chaim, M. Levin, A. Shlayer, and C. Estournes, Adv. Appl. Ceram. **107**, 159 (2008).
[178]R. Orrù, R. Licheri, A. M. Locci, A. Cincotti, and G. Cao, Mater. Sci. Eng.: R **63**, 127 (2009).
[179]J. Guo, H. Guo, A. L. Baker, M. T. Lanagan, E. R. Kupp, G. L. Messing, and C. A. Randall, Angew. Chem., Int. Ed. **55**, 11457 (2016).
[180]C. C. Liang, J. Electrochem. Soc. **120**, 1289 (1973).
[181]E. P. Butler and J. Drennan, J. Am. Ceram. Soc. **65**, 474 (1982).
[182]X. Guo, C.-Q. Tang, and R.-Z. Yuan, J. Eur. Ceram. Soc. **15**, 25 (1995).
[183]X. Guo and R.-Z. Yuan, Solid State Ionics **80**, 159 (1995).
[184]T. S. Zhang, J. Ma, L. B. Kong, S. H. Chan, P. Hing, and J. A. Kilner, Solid State Ionics **167**, 203 (2004).
[185]H. Aono, E. Sugimoto, Y. Sadaoka, N. Imanaka, and G. Adachi, J. Electrochem. Soc. **137**, 1023 (1990).
[186]H. Aono, E. Sugimoto, Y. Sadaoka, N. Imanaka, and G. Adachi, Solid State Ionics **47**, 257 (1991).
[187]G. Harley, R. Yu, and L. C. de Jonghe, Solid State Ionics **178**, 769 (2007).
[188]Y. Sadaoka, M. Matsuguchi, Y. Sakai, and S. Nakayama, J. Mater. Sci. **24**, 1299 (1989).
[189]T. Honma, M. Okamoto, T. Togashi, N. Ito, K. Shinozaki, and T. Komatsu, Solid State Ionics **269**, 19 (2015).
[190]K. Okubo, H. Wang, K. Hayashi, M. Inada, N. Enomoto, G. Hasegawa, T. Osawa, and H. Takamura, Electrochim. Acta **278**, 176 (2018).
[191]D. Chen, F. Luo, L. Gao, W. Zhou, and D. Zhu, J. Electron. Mater. **46**, 6367 (2017).
[192]K. Noi, K. Suzuki, N. Tanibata, A. Hayashi, and M. Tatsumisago, J. Am. Ceram. Soc. **101**, 1255 (2018).
[193]K. Suzuki, K. Noi, A. Hayashi, and M. Tatsumisago, Scr. Mater. **145**, 67 (2018).
[194]H. Leng, J. Nie, and J. Luo, J. Materiom. **5**, 237 (2019).
[195]J. A. S. Oh, L. He, A. Plewa, M. Morita, Y. Zhao, T. Sakamoto, X. Song, W. Zhai, K. Zeng, and L. Lu, ACS Appl. Mater. Interfaces **11**, 40125 (2019).
[196]Y. Zhao, C. Wang, Y. Dai, and H. Jin, Nano Energy **88**, 106293 (2021).
[197]Y. Ji, T. Honma, and T. Komatsu, Materials **14**, 3790 (2021).
[198]B. Santhoshkumar, M. B. Choudhary, A. K. Bera, S. M. Yusuf, M. Ghosh, and B. Pahari, J. Am. Ceram. Soc. **105**, 5011 (2022).
[199]A. M. Glass, K. Nassau, and T. J. Negran, J. Appl. Phys. **49**, 4808 (1978).
[200]B. V. R. Chowdari and K. Radhakrishnan, J. Non-Cryst. Solids **110**, 101 (1989).
[201]T. Honma, D. Oku, and T. Komatsu, Solid State Ionics **180**, 1457 (2009).
[202]N. Ohta, K. Takada, I. Sakaguchi, L. Zhang, R. Ma, K. Fukuda, M. Osada, and T. Sasaki, Electrochem. Commun. **9**, 1486 (2007).
[203]K. Takada, N. Ohta, L. Zhang, X. Xu, B. T. Hang, T. Ohnishi, M. Osada, and T. Sasaki, Solid State Ionics **225**, 594 (2012).
[204]J. Haruyama, K. Sodeyama, L. Han, K. Takada, and Y. Tateyama, Chem. Mater. **26**, 4248 (2014).
[205]K. Hayashi, K. Shima, and F. Sugiyama, J. Electrochem. Soc. **160**, A1467 (2013).
[206]M. M. Gross and A. Manthiram, ACS Appl. Energy Mater. **2**, 3445 (2019).
[207]S. Lanfredi, L. Dessemond, and A. C. M. Rodrigues, J. Am. Ceram. Soc. **86**, 291 (2003).
[208]S. K. Roy, S. N. Singh, K. Kumar, and K. Prasad, Adv. Mater. Res. **2**, 173 (2013).
[209]G. Gouget, M. Duttine, U.-C. Chung, S. Fourcade, F. Mauvy, M.-D. Braida, T. le Mercier, and A. Demourgues, Chem. Mater. **31**, 2828 (2019).
[210]A. Loutati, Y. J. Sohn, and F. Tietz, ChemPhysChem **22**, 995 (2021).
[211]S. F. Corbin and P. S. Apté, J. Am. Ceram. Soc. **82**, 1693 (1999).
[212]E. Chevalier, D. Chulia, C. Pouget, and M. Viana, J. Pharm. Sci. **97**, 1135 (2008).
[213]C. J. Brinker, Y. Lu, A. Sellinger, and H. Fan, Adv. Mater. **11**, 579 (1999).
[214]V. Malgras, H. Ataee-Esfahani, H. Wang, B. Jiang, C. Li, K. C.-W. Wu, J. H. Kim, and Y. Yamauchi, Adv. Mater. **28**, 993 (2016).
[215]A. Stein, B. E. Wilson, and S. G. Rudisill, Chem. Soc. Rev. **42**, 2763 (2013).
[216]A. Feinle, M. S. Elsaesser, and N. Hüsing, Chem. Soc. Rev. **45**, 3377 (2016).
[217]G. Hasegawa, K. Kanamori, and K. Nakanishi, J. Am. Ceram. Soc. **105**, 5 (2022).
[218]G. Hasegawa, J. Sol-Gel Sci. Technol. **103**, 637 (2022).
[219]T. Ohzuku, A. Ueda, and N. Yamamoto, J. Electrochem. Soc. **142**, 1431 (1995).
[220]M. M. Thackeray, J. Electrochem. Soc. **142**, 2558 (1995).
[221]Y. Wang, X. Yu, S. Xu, J. Bai, R. Xiao, Y.-S. Hu, H. Li, X.-Q. Yang, L. Chen, and X. Huang, Nat. Commun. **4**, 2365 (2013).
[222]Y. Cao, Q. Zhang, Y. Wei, Y. Guo, Z. Zhang, W. Huang, K. Yang, W. Chen, T. Zhai, H. Li, and Y. Cui, Adv. Funct. Mater. **30**, 1907023 (2020).
[223]Z. Wu, Y. Ni, S. Tan, E. Hu, L. He, J. Liu, M. Hou, P. Jiao, K. Zhang, F. Cheng, and J. Chen, J. Am. Chem. Soc. **145**, 9596 (2023).
[224]S. Chu, C. Zhang, H. Xu, S. Guo, P. Wang, and H. Zhou, Angew. Chem., Int. Ed. **60**, 13366 (2021).

[225]Y. Shi, Z. Zhang, P. Jiang, A. Gao, K. Li, Q. Zhang, Y. Sun, X. Lu, D. Cao, and X. Lu, Energy Storage Mater. **37**, 354 (2021).
[226]X. Zhang, D. Yu, Z. Wei, N. Chen, G. Chen, Z. X. Shen, and F. Du, ACS Appl. Mater. Interfaces **13**, 18897 (2021).
[227]H. Ren, L. Zheng, Y. Li, Q. Ni, J. Qian, Y. Li, Q. Li, M. Liu, Y. Bai, S. Weng, X. Wang, F. Wu, and C. Wu, Nano Energy **103**, 107765 (2022).
[228]Y. Huang, Y. Zhu, A. Nie, H. Fu, Z. Hu, X. Sun, S.-C. Haw, J.-M. Chen, T.-S. Chan, S. Yu, G. Sun, G. Jiang, J. Han, W. Luo, and Y. Huang, Adv. Mater. **34**, 2105404 (2022).
[229]C. D. Wessells, R. A. Huggins, and Y. Cui, Nat. Commun. **2**, 550 (2011).
[230]Y. Lu, L. Wang, J. Cheng, and J. B. Goodenough, Chem. Commun. **48**, 6544 (2012).
[231]L. Wang, Y. Lu, J. Liu, M. Xu, J. Cheng, D. Zhang, and J. B. Goodenough, Angew. Chem., Int. Ed. **52**, 1964 (2013).
[232]Y. You, X.-L. Wu, Y.-X. Yin, and Y.-G. Guo, J. Mater. Chem. A **1**, 14061 (2013).
[233]J. Qian, C. Wu, Y. Cao, Z. Ma, Y. Huang, X. Ai, and H. Yang, Adv. Energy Mater. **8**, 1702619 (2018).
[234]Q. Liu, Z. Hu, M. Chen, C. Zou, H. Jin, S. Wang, S.-L. Chou, Y. Liu, and S.-X. Dou, Adv. Funct. Mater. **30**, 1909530 (2020).
[235]J. Kim, G. Yoon, M. H. Lee, H. Kim, S. Lee, and K. Kang, Chem. Mater. **29**, 7826 (2017).
[236]M. Chen, W. Hua, J. Xiao, D. Cortie, X. Guo, E. Wang, Q. Gu, Z. Hu, S. Indris, X.-L. Wang, S.-L. Chou, and S.-X. Dou, Angew. Chem., Int. Ed. **59**, 2449 (2020).
[237]J.-J. Braconnier, C. Delmas, C. Fouassier, and P. Hagenmuller, Mater. Res. Bull. **15**, 1797 (1980).
[238]C. Guhl, P. Kehne, Q. Ma, F. Tietz, P. Komissinskiy, W. Jaegermann, and R. Hausbrand, Electrochim. Acta **268**, 226 (2018).
[239]P. Kehne, C. Guhl, Q. Ma, F. Tietz, L. Alff, R. Hausbrand, and P. Komissinskiy, J. Power Sources **409**, 86 (2019).
[240]H. Kageyama, K. Hayashi, K. Maeda, J. P. Attfield, Z. Hiroi, J. M. Rondinelli, and K. R. Poeppelmeier, Nat. Commun. **9**, 772 (2018).
[241]H. Kim, I. Park, D.-H. Seo, S. Lee, S.-W. Kim, W. J. Kwon, Y.-U. Park, C. S. Kim, S. Jeon, and K. Kang, J. Am. Chem. Soc. **134**, 10369 (2012).
[242]M. Nose, H. Nakayama, K. Nobuhara, H. Yamaguchi, S. Nakanishi, and H. Iba, J. Power Sources **234**, 175 (2013).
[243]M. Nose, S. Shiotani, H. Nakayama, K. Nobuhara, S. Nakanishi, and H. Iba, Electrochem. Commun. **34**, 266 (2013).
[244]M. Chen, W. Hua, J. Xiao, D. Cortie, W. Chen, E. Wang, Z. Hu, Q. Gu, X. Wang, S. Indris, S.-L. Chou, and S.-X. Dou, Nat. Commun. **10**, 1480 (2019).
[245]S. Y. Lim, H. Kim, J. Chung, J. H. Lee, B. G. Kim, J.-J. Choi, K. Y. Chung, W. Cho, S.-J. Kim, W. A. Goddard III, Y. Jung, and J. W. Choi, Proc. Natl. Acad. Sci. U. S. A. **111**, 599 (2014).
[246]C. Deng and S. Zhang, ACS Appl. Mater. Interfaces **6**, 9111 (2014).
[247]J.-M. Le Meins, M.-P. Crosnier-Lopez, A. Hemon-Ribaud, and G. Courbion, J. Solid State Chem. **148**, 260 (1999).
[248]K. Chihara, A. Kitajou, I. D. Gocheva, S. Okada, and J. Yamaki, J. Power Sources **227**, 80 (2013).
[249]M. Bianchini, F. Fauth, N. Brisset, F. Weill, E. Suard, C. Masquelier, and L. Croguennec, Chem. Mater. **27**, 3009 (2015).
[250]M. Xu, P. Xiao, S. Stauffer, J. Song, G. Henkelman, and J. B. Goodenough, Chem. Mater. **26**, 3089 (2014).
[251]Y.-U. Park, D.-H. Seo, H. Kim, J. Kim, S. Lee, B. Kim, and K. Kang, Adv. Funct. Mater. **24**, 4603 (2014).
[252]Y. Qi, L. Mu, J. Zhao, Y.-S. Hu, H. Liu, and S. Dai, Angew. Chem., Int. Ed. **54**, 9911 (2015).
[253]C. Masquelier and L. Croguennec, Chem. Rev. **113**, 6552 (2013).
[254]Y. Fang, J. Zhang, L. Xiao, X. Ai, Y. Cao, and H. Yang, Adv. Sci. **4**, 1600392 (2017).
[255]B. Senthilkumar, C. Murugesan, L. Sharma, S. Lochab, and P. Barpanda, Small Methods **3**, 1800253 (2019).
[256]C. Delmas, F. Cherkaoui, A. Nadiri, and P. Hagenmuller, Mater. Res. Bull. **22**, 631 (1987).
[257]C. Delmas, A. Nadiri, and J. L. Soubeyroux, Solid State Ionics **28-30**, 419 (1988).
[258]J. Gopalakrishnan and K. K. Rangan, Chem. Mater. **4**, 745 (1992).
[259]H. Huang, S.-C. Yin, T. Kerr, N. Taylor, and L. F. Nazar, Adv. Mater. **14**, 1525 (2002).
[260]M. Y. Saïdi, J. Barker, H. Huang, J. L. Swoyer, and G. Adamson, Electrochem. Solid-State Lett. **5**, A149 (2002).
[261]L. S. Plashnitsa, E. Kobayashi, Y. Noguchi, S. Okada, and J. Yamaki, J. Electrochem. Soc. **157**, A536 (2010).
[262]Z. Jian, W. Han, X. Lu, H. Yang, Y.-S. Hu, J. Zhou, Z. Zhou, J. Li, W. Chen, D. Chen, and L. Chen, Adv. Energy Mater. **3**, 156 (2013).
[263]W. Song, X. Cao, Z. Wu, J. Chen, K. Huangfu, X. Wang, Y. Huang, and X. Ji, Phys. Chem. Chem. Phys. **16**, 17681 (2014).
[264]G. Hasegawa, Y. Akiyama, M. Tanaka, R. Ishikawa, H. Akamatsu, Y. Ikuhara, and K. Hayashi, ACS Appl. Energy Mater. **3**, 6824 (2020).
[265]Y. Noguchi, E. Kobayashi, L. S. Plashnitsa, S. Okada, and J. Yamaki, Electrochim. Acta **101**, 59 (2013).
[266]F. Lalère, J. B. Leriche, M. Courty, S. Boulineau, V. Viallet, C. Masquelier, and V. Seznec, J. Power Sources **247**, 975 (2014).
[267]T. Lan, C.-L. Tsai, F. Tietz, X.-K. Wei, M. Heggen, R. E. Dunin-Borkowski, R. Wang, Y. Xiao, Q. Ma, and O. Guillon, Nano Energy **65**, 104040 (2019).
[268]Q. Ma, C.-L. Tsai, X.-K. Wei, M. Heggen, F. Tietz, and J. T. S. Irvine, J. Mater. Chem. A **7**, 7766 (2019).
[269]Z. Zhang, S. Wenzel, Y. Zhu, J. Sann, L. Shen, J. Yang, X. Yao, Y.-S. Hu, C. Wolverton, H. Li, L. Chen, and J. Janek, ACS Appl. Mater. Interfaces **3**, 7427 (2020).
[270]C.-L. Tsai, T. Lan, C. Dellen, Y. Ling, Q. Ma, D. Fattakhova-Rohlfing, O. Guillon, and F. Tietz, J. Power Sources **476**, 228666 (2020).
[271]L. Shen, J. Yang, G. Liu, M. Avdeev, and X. Yao, Mater. Today Energy **20**, 100691 (2021).
[272]Z. Grady, Z. Fan, A. Ndayishimiye, and C. A. Randall, ACS Appl. Mater. Interfaces **13**, 48071 (2021).
[273]A. K. Padhi, K. S. Nanjundaswamy, and J. B. Goodenough, J. Electrochem. Soc. **144**, 1188 (1997).
[274]B. Kang and G. Ceder, Nature **458**, 190 (2009).
[275]A. Bielefeld, D. A. Weber, and J. Janek, J. Phys. Chem. C **123**, 1626 (2019).
[276]R. Elango, A. Nadeina, F. Cadiou, V. de Andrade, A. Demortière, M. Morcrette, and V. Seznec, J. Power Sources **488**, 229402 (2021).
[277]H. Wang, G. Hasegawa, Y. Akiyama, T. Yamamoto, A. Inoishi, H. Akamatsu, M. Inada, T. Ishihara, and K. Hayashi, Electrochim. Acta **305**, 197 (2019).
[278]S. A. Novikova, R. V. Larkovich, A. A. Chekannikov, T. L. Kulova, A. M. Skundin, and A. B. Yaroslavtsev, Inorg. Mater. **54**, 794 (2018).
[279]F. Han, T. Gao, Y. Zhu, K. J. Gaskell, and C. Wang, Adv. Mater. **27**, 3473 (2015).
[280]A. Inoishi, T. Omuta, E. Kobayashi, A. Kitajou, and S. Okada, Adv. Mater. Interfaces **4**, 1600942 (2017).
[281]B. Lee, E. Paek, D. Mitlin, and S. W. Lee, Chem. Rev. **119**, 5416 (2019).
[282]W. Zhou, Y. Li, S. Xin, and J. B. Goodenough, ACS Cent. Sci. **3**, 52 (2017).
[283]X. Miao, H. Di, X. Ge, D. Zhao, P. Wang, R. Wang, C. Wang, and L. Yin, Energy Storage Mater. **30**, 170 (2020).
[284]J. Yang, Z. Gao, T. Ferber, H. Zhang, C. Guhl, L. Yang, Y. Li, Z. Deng, P. Liu, C. Cheng, R. Che, W. Jaegermann, R. Hausbrand, and Y. Huang, J. Mater. Chem. A **8**, 7828 (2020).
[285]H. Fu, Q. Yin, Y. Huang, H. Sun, Y. Chen, R. Zhang, Q. Yu, L. Gu, J. Duan, and W. Luo, ACS Mater. Lett. **2**, 127 (2020).
[286]Z. Sun, Y. Zhao, Q. Ni, Y. Liu, C. Sun, J. Li, and H. Jin, Small **18**, 2200716 (2022).
[287]Z. Sun, L. Li, C. Sun, Q. Ni, Y. Zhao, H. Wu, and H. Jin, Nano Lett. **22**, 7187 (2022).
[288]Y. Lu, J. A. Alonso, Q. Yi, L. Lu, Z. L. Wang, and C. Sun, Adv. Energy Mater. **9**, 1901205 (2019).
[289]R. Raj and J. Wolfenstine, J. Power Sources **343**, 119 (2017).
[290]Z. Ning, D. S. Jolly, G. Li, R. de Meyere, S. D. Pu, Y. Chen, J. Kasemchainan, J. Ihli, C. Gong, B. Liu, D. L. R. Melvin, A. Bonnin, O. Magdysyuk, P. Adamson, G. O. Hartley, C. W. Monroe, T. J. Marrow, and P. G. Bruce, Nat. Mater. **20**, 1121 (2021).

[291]S. A. Pervez, E. P. L. Roberts, and M. Trifkovic, Energy Technol. **10**, 2200658 (2022).
[292]Y. Uchida, G. Hasegawa, K. Shima, M. Inada, N. Enomoto, H. Akamatsu, and K. Hayashi, ACS Appl. Energy Mater. **2**, 2913 (2019).
[293]G. Hasegawa, Y. Uchida, K. Shima, M. Inada, N. Enomoto, H. Akamatsu, and K. Hayashi, "Investigation of interfacial charge transfer between Na anode and solid electrolytes," in *5th Solid-State Chemistry and Ionics (SCI) workshop* (Nishijin Plaza, Fukuoka, Japan, 2018).
[294]M.-C. Bay, M. Wang, R. Grissa, M. V. F. Heinz, J. Sakamoto, and C. Battaglia, Adv. Energy Mater. **10**, 1902899 (2020).
[295]D. I. Iermakova, R. Dugas, M. R. Palacín, and A. Ponrouch, J. Electrochem. Soc. **162**, A7060 (2015).
[296]C. Zhao, Z. Sun, Y. Zhao, B. Wang, S. Shao, C. Sun, Y. Zhao, J. Li, and L. Qu, Small **17**, 2103819 (2021).
[297]Z. Yang, B. Tang, Z. Xie, and Z. Zhou, ChemElectroChem **8**, 1035 (2021).
[298]R. Sudo, Y. Nakata, K. Ishiguro, M. Matsui, A. Hirano, Y. Takeda, O. Yamamoto, and N. Imanishi, Solid State Ionics **262**, 151 (2014).
[299]Y. Ren, Y. Shen, Y. Lin, and C.-W. Nan, Electrochem. Commun. **57**, 27 (2015).
[300]L. Porz, T. Swamy, B. W. Sheldon, D. Rettenwander, T. Frömling, H. L. Thaman, S. Berendts, R. Uecker, W. C. Carter, and Y.-M. Chiang, Adv. Energy Mater. **7**, 1701003 (2017).
[301]E. J. Cheng, A. Sharafi, and J. Sakamoto, Electrochim. Acta **223**, 85 (2017).
[302]T. Swamy, R. Park, B. W. Sheldon, D. Rettenwander, L. Porz, S. Berendts, R. Uecker, W. C. Carter, and Y.-M. Chiang, J. Electrochem. Soc. **165**, A3648 (2018).
[303]Q. Ma, T. Ortmann, A. Yang, D. Sebold, S. Burkhardt, M. Rohnke, F. Tietz, D. Fattakhova-Rohlfing, J. Janek, and O. Guillon, Adv. Energy Mater. **12**, 2201680 (2022).
[304]F. Han, A. S. Westover, J. Yue, X. Fan, F. Wang, M. Chi, D. N. Leonard, N. J. Dudney, H. Wang, and C. Wang, Nat. Energy **4**, 187 (2019).
[305]L. Viswanathan and A. V. Virkar, J. Mater. Sci. **17**, 753 (1982).
[306]A. Sharafi, H. M. Meyer, J. Nanda, J. Wolfenstine, and J. Sakamoto, J. Power Sources **302**, 135 (2016).
[307]J. Kasemchainan, S. Zekoll, D. S. Jolly, Z. Ning, G. O. Hartley, J. Marrow, and P. G. Bruce, Nat. Mater. **18**, 1105 (2019).
[308]D. S. Jolly, Z. Ning, J. E. Darnbrough, J. Kasemchainan, G. O. Hartley, P. Adamson, D. E. J. Armstrong, J. Marrow, and P. G. Bruce, ACS Appl. Mater. Interfaces **12**, 678 (2020).
[309]A. Kubanska, L. Castro, L. Tortet, M. Dollé, and R. Bouchet, J. Electroceram. **38**, 189 (2017).
[310]Y. Kato, S. Shiotani, K. Morita, K. Suzuki, M. Hirayama, and R. Kanno, J. Phys. Chem. Lett. **9**, 607 (2018).
[311]C.-L. Tsai, Q. Ma, C. Dellen, S. Lobe, F. Vondahlen, A. Windmüller, D. Grüner, H. Zheng, S. Uhlenbruck, M. Finsterbusch, F. Tietz, D. Fattakhova-Rohlfing, H. P. Buchkremer, and O. Guillon, Sustainable Energy Fuels **3**, 280 (2019).
[312]A. P. Cohn, N. Muralidharan, R. Carter, K. Share, and C. L. Pint, Nano Lett. **17**, 1296 (2017).
[313]A. Wang, X. Hu, H. tang, C. Zhang, S. Liu, Y.-W. Yang, Q.-H. Yang, and J. Luo, Angew. Chem., Int. Ed. **56**, 11921 (2017).
[314]M. Dahbi, N. Yabuuchi, K. Kubota, K. Tokiwa, and S. Komaba, Phys. Chem. Chem. Phys. **16**, 15007 (2014).
[315]W. Luo, F. Shen, C. Bommier, H. Zhu, X. Ji, and L. Hu, Acc. Chem. Res. **49**, 231 (2016).
[316]M. Á. Muñoz-Márquez, D. Saurel, J. L. Gómez-Cámer, M. Casas-Cabanas, E. Castillo-Martínez, and T. Rojo, Adv. Energy Mater. **7**, 1700463 (2017).
[317]A. Kamiyama, K. Kubota, D. Igarashi, Y. Youn, Y. Tateyama, H. Ando, K. Gotoh, and S. Komaba, Angew. Chem., Int. Ed. **60**, 5114 (2021).
[318]D. A. Stevens and J. R. Dahn, J. Electrochem. Soc. **147**, 1271 (2000).
[319]B. Zhang, C. M. Ghimbeu, C. Laberty, C. Vix-Guterl, and J.-M. Tarascon, Adv. Energy Mater. **6**, 1501588 (2016).
[320]G. Hasegawa, K. Kanamori, N. Kannari, J. Ozaki, K. Nakanishi, and T. Abe, ChemElectroChem **2**, 1917 (2015).
[321]G. Hasegawa, K. Kanamori, N. Kannari, J. Ozaki, K. Nakanishi, and T. Abe, J. Power Sources **318**, 41 (2016).
[322]S. Komaba, W. Murata, T. Ishikawa, N. Yabuuchi, T. Ozeki, T. Nakayama, A. Ogata, K. Gotoh, and K. Fujiwara, Adv. Funct. Mater. **21**, 3859 (2011).
[323]K. Niitani, S. Ushiroda, H. Kuwata, H. N. Ohata, Y. Shimo, M. Hozumi, T. Matsunaga, and S. Nakanishi, ACS Energy Lett. **7**, 145 (2022).
[324]W. Wang, B. Jiang, L. Hu, and S. Jiao, J. Mater. Chem. A **2**, 1341 (2014).
[325]C. C. Liang, J. Epstein, and G. H. Boyle, J. Electrochem. Soc. **116**, 1452 (1969).
[326]C. C. Liang and P. Bro, J. Electrochem. Soc. **116**, 1322 (1969).
[327]M. L. B. Rao and B. Mass, U.S. patent 3455742 (10 February 1969).
[328]K. Kanehori, K. Matsumoto, K. Miyauchi, and T. Kudo, Solid State Ionics **9-10**, 1445 (1983).
[329]P. Birke, F. Salam, S. Döring, and W. Weppner, Solid State Ionics **118**, 149 (1999).
[330]Z. Siroma, T. Sato, T. Takeuchi, R. Nagai, A. Ota, and T. Ioroi, J. Power Sources **316**, 215 (2016).
[331]T. Asano, S. Yubuchi, A. Sakuda, A. Hayashi, and M. Tatsumisago, J. Electrochem. Soc. **164**, A3960 (2017).
[332]N. Kaiser, S. Spannenberger, M. Schmitt, M. Cronau, Y. Kato, and B. Roling, J. Power Sources **396**, 175 (2018).
[333]F. Shen, M. B. Dixit, W. Zaman, N. Hortance, B. Rogers, and K. B. Hatzell, J. Electrochem. Soc. **166**, A3182 (2019).
[334]J. Park, K. T. Kim, D. Y. Oh, D. Jin, D. Kim, Y. S. Jung, and Y. M. Lee, Adv. Energy Mater. **10**, 2001563 (2020).
[335]T. Shi, Q. Tu, Y. Tian, Y. Xiao, L. J. Miara, O. Kononova, and G. Ceder, Adv. Energy Mater. **10**, 1902881 (2020).
[336]P. Minnmann, L. Quillman, S. Burkhardt, F. H. Richter, and J. Janek, J. Electrochem. Soc. **168**, 040537 (2021).
[337]P. Barai, T. Rojas, B. Narayanan, A. T. Ngo, L. A. Curtiss, and V. Srinivasan, Chem. Mater. **33**, 5527 (2021).
[338]T. Kato, R. Yoshida, K. Yamamoto, T. Hirayama, M. Motoyama, W. C. West, and Y. Iriyama, J. Power Sources **325**, 584 (2016).
[339]K. J. Kim and J. L. M. Rupp, Energy Environ. Sci. **13**, 4930 (2020).
[340]Y. Zhu, X. He, and Y. Mo, J. Mater. Chem. A **4**, 3253 (2016).
[341]R. Koerver, F. Walther, I. Aygün, J. Sann, C. Dietrich, W. G. Zeier, and J. Janek, J. Mater. Chem. A **5**, 22750 (2017).
[342]A. A. Delluva, J. Kulberg-Savercool, and A. Holewinski, Adv. Funct. Mater. **31**, 2103716 (2021).
[343]S. Lou, F. Zhang, C. Fu, M. Chen, Y. Ma, G. Yin, and J. Wang, Adv. Mater. **33**, 2000721 (2021).
[344]A. Banerjee, X. Wang, C. Fang, E. A. Wu, and Y. S. Meng, Chem. Rev. **120**, 6878 (2020).
[345]Y. Xiao, Y. Wang, S.-H. Bo, J. C. Kim, L. J. Miara, and G. Ceder, Nat. Rev. Mater. **5**, 105 (2020).
[346]S. Ito, S. Fujiki, T. Yamada, Y. Aihara, Y. Park, T. Y. Kim, S.-W. Baek, J.-M. Lee, S. Doo, and N. Machida, J. Power Sources **248**, 943 (2014).
[347]K. Okada, N. Machida, M. Naito, T. Shigematsu, S. Ito, S. Fujiki, M. Nakano, and Y. Aihara, Solid State Ionics **255**, 120 (2014).
[348]S. H. Jung, K. Oh, Y. J. Nam, D. Y. Oh, P. Brüner, K. Kang, and Y. S. Jung, Chem. Mater. **30**, 8190 (2018).
[349]K. Heo, J. Lee, J. Im, M.-Y. Kim, H.-S. Kim, D. Ahn, J. Kim, and J. Lim, J. Mater. Chem. A **8**, 22893 (2020).
[350]J. S. Lee and Y. J. Park, ACS Appl. Mater. Interfaces **13**, 38333 (2021).
[351]Y. Wang, Y. Lv, L. Chen, H. Li, and F. Wu, Nano Energy **90**, 106589 (2021).
[352]Y. Ma, J. H. Teo, F. Walther, Y. Ma, R. Zhang, A. Mazilkin, Y. Tang, D. Goonetilleke, J. Janek, M. Bianchini, and T. Brezesinski, Adv. Funct. Mater. **32**, 2111829 (2022).
[353]X. Sun, L. Wang, J. Ma, X. Yu, S. Zhang, X. Zhou, and G. Cui, ACS Appl. Mater. Interfaces **14**, 17674 (2022).
[354]S. P. Culver, R. Koerver, W. G. Zeier, and J. Janek, Adv. Energy Mater. **9**, 1900626 (2019).
[355]S. Jamil, G. Wang, M. Fasehullah, and M. Xu, J. Alloys Compd. **909**, 164727 (2022).
[356]S. Ohta, S. Komagata, J. Seki, T. Saeki, S. Morishita, and T. Asaoka, J. Power Sources **238**, 53 (2013).
[357]Y. J. Nam, D. Y. Oh, S. H. Jung, and Y. S. Jung, J. Power Sources **375**, 93 (2018).
[358]S. Jia, S. Ohno, J. Wang, G. Hasegawa, H. Akamatsu, and K. Hayashi, ACS Appl. Energy Mater. **6**, 317 (2023).

[359]A. Roosen, J. Eur. Ceram. Soc. **21**, 1993 (2001).
[360]J. Gurauskis, A. J. Sánchez-Herencia, and C. Baudín, J. Eur. Ceram. Soc. **25**, 3403 (2005).
[361]D. Jurkow, H. Roguszczak, and L. Golonka, J. Eur. Ceram. Soc. **29**, 703 (2009).
[362]T. Kobayashi, F. Chen, V. Seznec, and C. Masquelier, J. Power Sources **450**, 227597 (2020).
[363]X. Zhang, E. Temeche, and R. M. Laine, Macromolecules **53**, 2702 (2020).
[364]A. Atkinson and A. Selçuk, Acta Mater. **47**, 867 (1999).
[365]S.-H. Lee, G. L. Messing, and M. Awano, J. Am. Ceram. Soc. **91**, 421 (2008).
[366]M. Bertrand, S. Rousselot, D. Aymé-Perrot, and M. Dollé, Mater. Adv. **2**, 2989 (2021).
[367]H. Zhang, X. Liu, Y. Qi, and V. Liu, J. Alloys Compd. **577**, 57 (2013).
[368]M. Zhang, Z. Huang, J. Cheng, O. Yamamoto, N. Imanishi, B. Chi, J. Pu, and J. Li, J. Alloys Compd. **590**, 147 (2014).
[369]T. Wei, Y. Gong, X. Zhao, and K. Huang, Adv. Funct. Mater. **24**, 5380 (2014).
[370]E. Yi, W. Wang, J. Kieffer, and R. M. Laine, J. Mater. Chem. A **4**, 12947 (2016).
[371]R. Jiménez, A. del Campo, M. L. Calzada, J. Sanz, S. D. Kobylianska, S. O. Solopan, and A. G. Belous, J. Electrochem. Soc. **163**, A1653 (2016).
[372]F. Schröckert, N. Schiffmann, E. C. Bucharsky, K. G. Schell, and M. J. Hoffmann, Solid State Ionics **328**, 25 (2018).
[373]V. A. Vizgalov, A. R. Lukovkina, D. M. Itkis, and L. V. Yashina, J. Mater. Sci. **54**, 8531 (2019).
[374]A. Paolella, W. Zhu, G.-L. Xu, A. la Monaca, S. Savoie, G. Girard, A. Vijh, H. Demers, A. Perea, N. Delaporte, A. Guerfi, X. Liu, Y. Ren, C.-J. Sun, J. Lu, K. Amine, and K. Zaghib, Adv. Energy Mater. **10**, 2001497 (2020).
[375]Z. Jiang, S. Wang, X. Chen, W. Yang, X. Yao, X. Hu, Q. Han, and H. Wang, Adv. Mater. **32**, 1906221 (2020).
[376]B. Emley, Y. Liang, R. Chen, C. Wu, M. Pan, Z. Fan, and Y. Yao, Mater. Today Phys. **18**, 100397 (2021).
[377]A. Yang, R. Ye, X. Li, Q. Lu, H. Song, D. Grüner, Q. Ma, F. Tietz, D. Fattakhova-Rohlfing, and O. Guillon, Chem. Eng. J. **435**, 134774 (2022).
[378]N. Li, Z. Wen, Y. Liu, X. Xu, J. Lin, and Z. Gu, J. Eur. Ceram. Soc. **29**, 3031 (2009).
[379]S. C. Ligon, M.-C. Bay, M. V. F. Heinz, C. Battaglia, T. Graule, and G. Blugan, Materials **13**, 433 (2020).
[380]T. Kashihara, G. Hasegawa, H. Akamatsu, and K. Hayashi, "Preparation of oxide-based Na ion battery by tape-casting laminate NASICON-type ceramics," in *13th Pacific Rim Conference of Ceramic Societies (PACRIM13)* (Okinawa Convention Center, Okinawa, Japan, 2019).
[381]Y.-K. Sun, S.-T. Myung, B.-C. Park, J. Prakash, I. Belharouak, and K. Amine, Nat. Mater. **8**, 320 (2009).
[382]J. Y. Kim, J. Kim, S. H. Kang, D. O. Shin, M. J. Lee, J. Oh, Y.-G. Lee, and K. M. Kim, ETRI J. **42**, 129 (2020).
[383]J. Y. Kim, S. Jung, S. H. Kang, M. J. Lee, D. Jin, D. O. Shin, Y.-G. Lee, and Y. M. Lee, J. Power Sources **518**, 230736 (2022).
[384]J.-G. Yeo, Y.-G. Jung, and S.-C. Choi, Mater. Lett. **37**, 304 (1998).
[385]N. C. Acikbas, E. Suvaci, and H. Mandal, J. Am. Ceram. Soc. **89**, 3255 (2006).
[386]I. Riess, Solid State Ionics **157**, 1 (2003).
[387]S. Kikkawa, S. Miyazaki, and M. Koizumi, J. Power Sources **14**, 231 (1985).
[388]W. Schmidt, P. Bottke, M. Sternad, P. Gollob, V. Hennige, and M. Wilkening, Chem. Mater. **27**, 1740 (2015).
[389]J. Molenda, Solid State Ionics **21**, 263 (1986).